

Department of Physics and Astronomy
University of Heidelberg

Bachelor Thesis in Physics
submitted by

Alexander Erb

born in Frankfurt a.M. (Germany)

2018

Infrared Spectroscopy of Plasmonic Antennas and Multilayer Systems

This Bachelor Thesis has been carried out by Alexander Erb at the
Kirchhoff Institute for Physics in Heidelberg
under the supervision of
Prof. Dr. Na Liu

Abstract

Metal nanoantennas, when exposed to electromagnetic radiation, show a decreased relative transmission for specific frequencies. This behavior is due to plasmonic excitations. The plasmonic resonance frequency is strongly dependent on antenna length, width and height as well as the material. Varying these parameters resonances can be tuned for applications in surfaced enhanced infrared spectroscopy.

In this work such an optimization was carried out for enhancement of DNA, HMDS and amide I protein group vibrational signals. Gold, aluminum, copper and magnesium nanoantennas were used. Furthermore, multilayer systems of gold on top of aluminum, copper or magnesium were simulated and measured using Fourier transform spectroscopy.

Zusammenfassung

Unter Bestrahlung mit infrarotem Licht zeigen Nanoantennen eine stark verringerte Transmission für bestimmte Frequenzbereiche. Grund dafür sind plasmonische Anregungen. Die Resonanzfrequenz dieser Anregung wird durch Höhe, Breite und Länge der Antenne sowie durch das Material bestimmt. Durch Änderung dieser Parameter ist eine Optimierung für oberflächenverstärkte Infrarotspektroskopie möglich.

In dieser Arbeit wurde eine solche Optimierung für die Infrarotsignale von DNA, HMDS und einer Protein Amide I Gruppe durchgeführt. Als Materialien wurden Gold, Aluminium, Kupfer und Magnesium verwendet. Zusätzlich wurden Zweischichtsysteme aus Gold auf Aluminium, Kupfer oder Magnesium simuliert und vermessen.

Contents

1 Introduction

Metal nanoparticles have been in use for centuries, but only in the last decade scientists started to understand the concepts leading to the fundamental properties of these interesting particles.

Especially the field of nanoantennas recently gained a lot of attention for the various applications in biology, imaging and sensing [?].

One of the promising sensing applications is called 'surface-enhanced infrared spectroscopy using resonant nanoantennas' (SEIRS). It was first introduced by Neubrech et al. in 2008 [?] while the concept of using metal structures for surface enhanced infrared spectroscopy was already expressed by Hartstein et. al in 1980 [?].

Infrared spectroscopy in general is a powerful spectroscopic tool with many advantages: It is label-free and leads to a precise identification of molecular substances. Therefore it is widely used in research and industry. From vibration reaction extracted information include chemical bonds, molecular setup as well as configuration. Some examples of specific vibrational frequencies of selected materials are shown in figure ??.

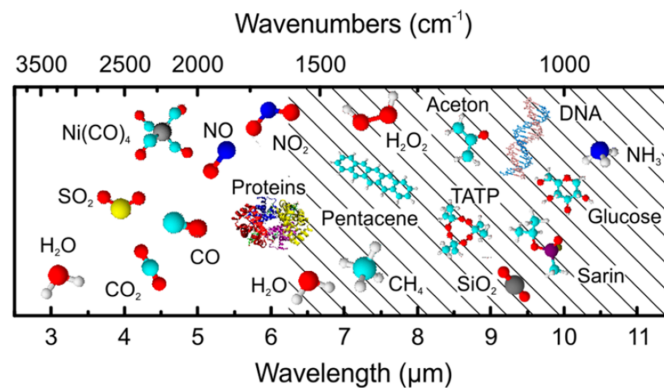


Figure 1: Characteristic wavenumbers for different molecules. Note that almost all shown examples have their characteristic resonance in the infrared regime (1000cm^{-1} to 2500cm^{-1}). Graphic taken from [?].

Generally speaking a nanoantenna is a rectangular solid produced on a certain substrate with a set material, height, width and length with sub-wavelength dimensions. It can be driven using incident electromagnetic radiation and will respond with reso-

1. Introduction

nances for certain frequencies depending on its geometry. Nanoantennas for enhancement are needed due to the low absorption cross-sections of mid-infrared vibrations ($\sigma_{abs} \approx 10^{-20} \text{cm}^2$) of molecules. Thus, a large amount of material is needed to be able to conduct infrared spectroscopy which is not always possible. In the process localized surface plasmons polariton resonances (LSPRs) which can also be described as surface plasmon polaritons (SPPs) are stimulated. They are strongly geometry and material depended and have a resonant excitation that comes with enhanced electromagnetic near-fields which can be used for surface enhanced light-matter interactions such as SEIR. Hence, enhancements up to approximately 5 orders of magnitude (for sharp LSPRs) are possible. In figure ?? such an enhanced signal is shown.

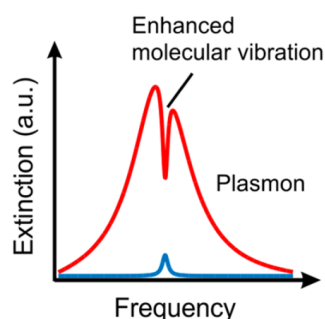


Figure 2: Principle of SEIRA: Plasmon resonance (red) is matched to molecule vibration (blue). Molecule resonance is enhanced as it can be seen in the plasmon curve (red). (graphic taken from [?])

The objective of this thesis is the tuning and investigation of nanoantennas and multilayer nanoantenna systems for future application in the field of nanoantenna enhanced infrared spectroscopy. It is planned to add gold caps to both short ends of a Copper, Aluminum and Magnesium nanoantenna. There a functionalization with DNA via sulfur-gold binding is attached. Using DNA origami other materials can be added resulting in a selectivity of material to be sensed. Here, Streptavidin (STV) a protein contained in many bacteria will be added via its amide I group. To make sure the hydrophilic DNA and protein don't stick to the substrate calcium fluoride (CaF_2) a hydrophobic layer of Hexamethyldisilazane (HMDS) covers the surface. In this thesis optimization was done for the main vibrational bands of DNA, (HMDS) and a protein amide I group. A schematic plot of the described setup is shown in figure ?? a). Also the main vibrational bands of DNA, HMDS, and protein amide I group are shown.

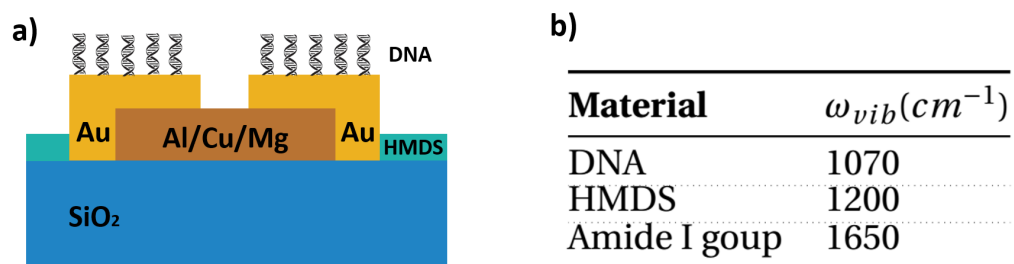


Figure 3: a) Plan for future setup of a nanoantenna enhanced infrared spectroscopy. b) vibrational bands of selected materials.

2 Theoretical Background

In this chapter the related theoretical physics for this thesis will be presented. First Maxwell's equations will be used to derive some important relations in plasmonics. In the second part Drude's model will be presented and further analyzed. Then Plasmon polaritons of different categories (bulk, surface and particle) will be discussed. After that behavior of single and periodically arranged nanoantennas upon electromagnetic excitation will be analyzed. In the last part the working principles of infrared spectroscopy as well as some basic concepts of surface enhanced infrared absorption will be presented.

Please note that bold text is used to indicate vector character of properties in this thesis.

2.1 Maxwell's equations

Maxwell's equations are the fundamental set of equations for classical electrodynamics. Derived by Maxwell and summarized into four basic formulas by Oliver Heaviside in 1884 these differential equations come in two forms - integral and differential. Both can be transferred to each other by using Gauss's theorem and Stokes' theorem. In this thesis, mainly the equations in differential form will be used (in SI units).

$$\begin{aligned}\operatorname{div}(\mathbf{E}) &= \frac{\rho}{\epsilon_0} \\ \operatorname{div}(\mathbf{B}) &= 0 \\ \operatorname{rot}(\mathbf{E}) &= -\frac{\partial \mathbf{B}}{\partial t} \\ \operatorname{rot}(\mathbf{B}) &= \mu_0 \left(\mathbf{J} + \epsilon_0 \frac{\partial \mathbf{E}}{\partial t} \right)\end{aligned}\tag{1}$$

Here, \mathbf{E} is the electric field, \mathbf{B} is the magnetic flux density, t is the time \mathbf{J} the current density, ρ the charge density, μ_0 the vacuum permeability and ϵ_0 the vacuum permittivity.

For macroscopic setups Maxwell's equations have to be adjusted using the displace-

ment field $\mathbf{D} = \varepsilon_0 \varepsilon \mathbf{E}$ and the magnetizing field $\mathbf{H} = \frac{1}{\mu_0 \mu} \mathbf{B}$. While the second and third equation remain the same, the first and fourth have to be adjusted

$$\begin{aligned} \operatorname{div}(\mathbf{D}) &= \rho_{free} \\ \operatorname{rot}(\mathbf{H}) &= \mathbf{J}_{free} + \frac{\partial \mathbf{D}}{\partial t} \end{aligned} \quad (2)$$

Using the ansatz $\Delta \mathbf{E} = \operatorname{grad}(\operatorname{div}(\mathbf{E})) - \operatorname{rot}(\operatorname{rot}(\mathbf{E}))$ one comes to the so called Telegrapher's equations

$$\Delta \mathbf{E} = \operatorname{grad}(\operatorname{div}(\mathbf{E})) + \frac{\varepsilon}{c^2} \frac{\partial^2 \mathbf{E}}{\partial t^2} \quad (3)$$

Here it is assumed due to the fact that only non magnetic materials are considered that $\mu_0 \approx 1$ and in addition that $\mathbf{J}_{free} \approx 0$. It is also used that per definition $\mu_0 \varepsilon_0 = \frac{1}{c^2}$ with the vacuum speed of light c .

Now the electrical field of a propagating electromagnetic wave is used

$$\mathbf{E} = E_0 \exp(i[\mathbf{k}\mathbf{x} - \omega t]) \quad (4)$$

Now using the relation $\operatorname{div}(\mathbf{E}) = i(k_x + k_y + k_z)\mathbf{E} = i\mathbf{k}\mathbf{E}$, $\operatorname{grad}(\mathbf{E}) = i\mathbf{k}\mathbf{E}$ and $\frac{\partial^2 \mathbf{E}}{\partial t^2} = -\omega^2 \mathbf{E}$ as well as $\Delta \mathbf{E} = -\mathbf{k}^2 \mathbf{E} = k^2 \mathbf{E}$ one ends up with the following relation

$$k^2 \mathbf{E} = \mathbf{k}(\mathbf{k} \cdot \mathbf{E}) + \frac{\varepsilon \omega^2}{c^2} \mathbf{E} \quad (5)$$

This equation is called *wave equation* and gives an important dispersion relation for electromagnetic waves.

For transverse waves the wavevector \mathbf{k} and the electric field of the incident light \mathbf{E} are perpendicular to each other so that

$$\begin{aligned} \mathbf{k} \cdot \mathbf{E} &= 0 \\ \Rightarrow k^2 &= \frac{\varepsilon \omega^2}{c^2} \end{aligned} \quad (6)$$

2.2 Drude model

Drudes model, evolved in 1900 [?], is a widely used model for the description of optical properties of metals. It is based on the assumption that movement of electrons in the conduction band can be described using the kinetic gas theory. All electrons are assumed to move freely. All electron electron interactions as well as collisions with ionic cores are neglected. Only interaction between electrons and defects as well as phonons are taken into account resulting in an resistance.

The classical equation of movement for an electron of charge e and effective mass m_e in an external electrical field E_{ext} is then given by

$$m_e \ddot{\mathbf{r}}(t) = e \mathbf{E}_{ext} - m_e \Gamma \dot{\mathbf{r}}(t) \quad (7)$$

Here, $\dot{\mathbf{r}}(t)$ is the drift velocity and $\Gamma = 1/\tau$ is the inverse mean free time between collisions also called relaxationrate ω_τ , τ is called relaxation time. The last term corresponds to the before described damping.

Using the ansatz $\mathbf{r} = \mathbf{r}_0 \exp(-i\omega t)$ one gets to the following equation

$$\mathbf{r}(t) = \frac{e}{m_e(\omega^2 + i\omega\Gamma)} \mathbf{E} \quad (8)$$

Knowing that $\mathbf{D} = \epsilon_0 \mathbf{E} + \mathbf{P} = \epsilon_0 \mathbf{E} - n e \mathbf{r}$ where n denotes the electron density and introducing the plasma frequency

$$\omega_p = \sqrt{\frac{e^2 n}{\epsilon_0 m_e}} \quad (9)$$

one ends up with the following displacement field

$$\mathbf{D} = \epsilon_0 \left(1 - \frac{\omega_p^2}{\omega^2 + i\omega\Gamma} \right) \cdot \mathbf{E} \quad (10)$$

Since $\mathbf{D} = \epsilon_0 \epsilon(\omega) \mathbf{E}$ the (complex) dielectric function for a free electron gas can be ex-

tracted to be

$$\epsilon(\omega) = 1 - \frac{\omega_p^2}{\omega^2 + i\omega\Gamma} \quad (11)$$

Analyzing equation ?? it becomes clear, that one can describe a Drude metal by just two parameters - the plasma frequency ω_p and the damping Γ . ω_p is directly related to the electron density in the metal while Γ is mainly caused by defects and boundaries. Typical values for the here used materials are shown in table ??.

	$\omega_p(\text{cm}^{-1})$	$\Gamma(\text{cm}^{-1})$
Au	72400	215
Al	11900	660
Cu	59600	73

Table 1: Bulk material properties as used for simulations. Data taken from [?].

In figure ?? the dielectric functions of Gold (Au), Aluminum (Al), Copper (Cu) and Magnesium (Mg) are shown. Note, only the first 3 dielectric functions are described by the Drude model. All Drude parameters were chosen as shown in table ?. For Mg the shown data points were extracted from [?].

Plasma Frequency As seen before the plasma frequency (see equation ??) is a material constant only depending on the electron density n and effective electron mass m_e .

Assuming zero damping $\Gamma = 0$ equation ?? simplifies to

$$\epsilon(\omega) = 1 - \frac{\omega_p^2}{\omega^2} \quad (12)$$

It is easy to see that ω_p is exactly the frequency where $\epsilon = 0$ (see figure ?? a). For $\omega > \omega_p$ the dielectric function becomes positive enabling the propagation of transverse electromagnetic waves.

For further study of the plasma frequency we will use the complex refractive index $n = \sqrt{\epsilon\mu} = n' + i\kappa$ as well as the following formula for the reflectivity of a metal air surface

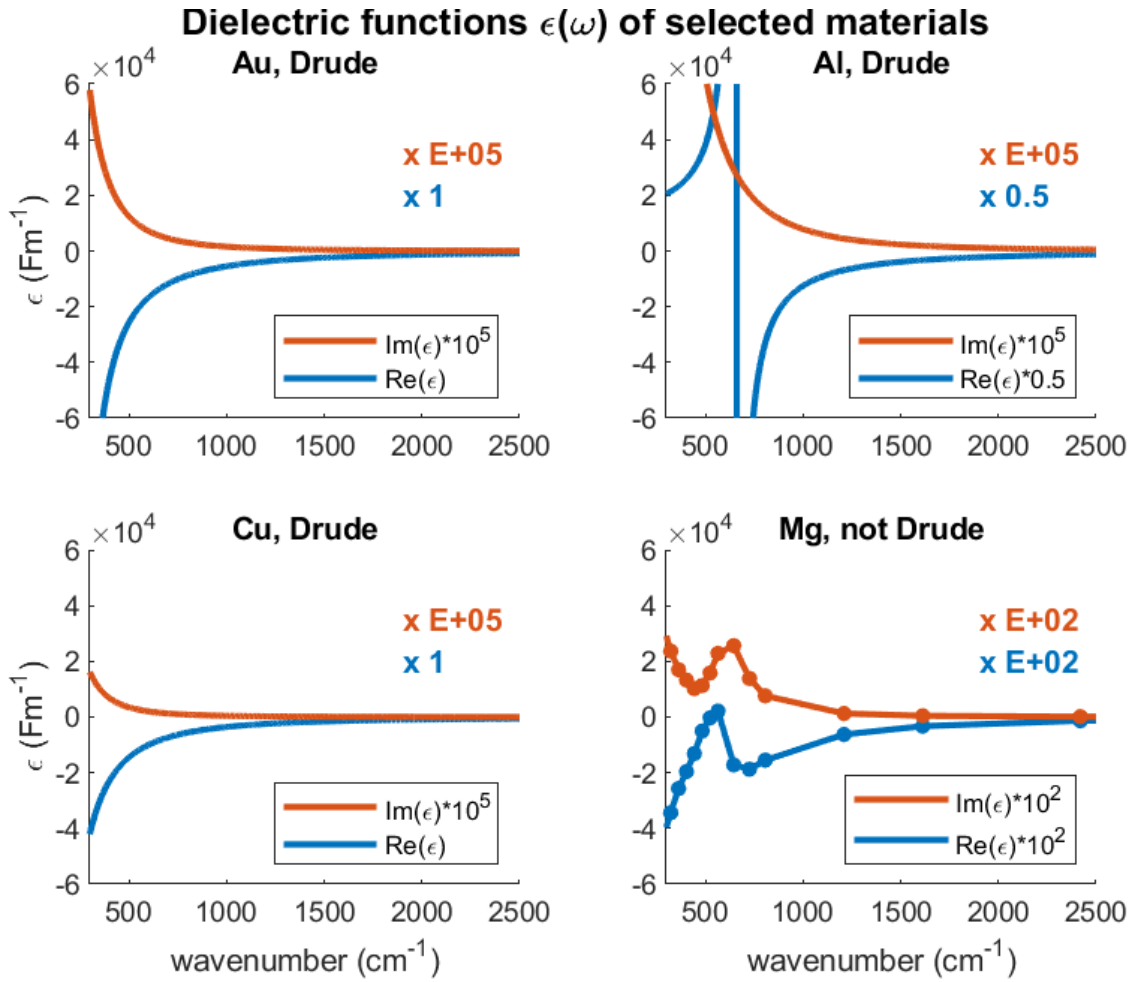


Figure 4: Dielectric functions of Gold (Au), Aluminum (Al) and Copper (Cu) as obtained using the Drude parameters shown in table ???. Data extracted from [?]. In red the real part of the permittivity $Re(\epsilon)$, in blue the imaginary part $Im(\epsilon)$ is shown. Note, that some curves are enhanced as indicated by the enhancement factors on the upper right of each spectrum. For Magnesium measured data was extracted from [?].

under normal incident light with zero damping ($\kappa = 0$)

$$R = \left| \frac{n' - 1}{n' + 1} \right|^2 \quad (13)$$

Resulting are the following 3 scenarios for the relectivity R

$$R = \begin{cases} 1 & \omega < \omega_p \Leftrightarrow \epsilon(\omega) < 0 \Leftrightarrow n' = 0 \\ 1 & \omega = \omega_p \Leftrightarrow \epsilon(\omega) = 0 \Leftrightarrow n' = 0 \\ 0 & \omega > \omega_p \Leftrightarrow \epsilon(\omega) > 0 \Leftrightarrow n' = 1 \end{cases}$$

This implicates that the plasma frequency is exactly the frequency a metal starts to allow electromagnetic radiation to pass it resulting in a decreased reflectivity (see figure ?? b)).

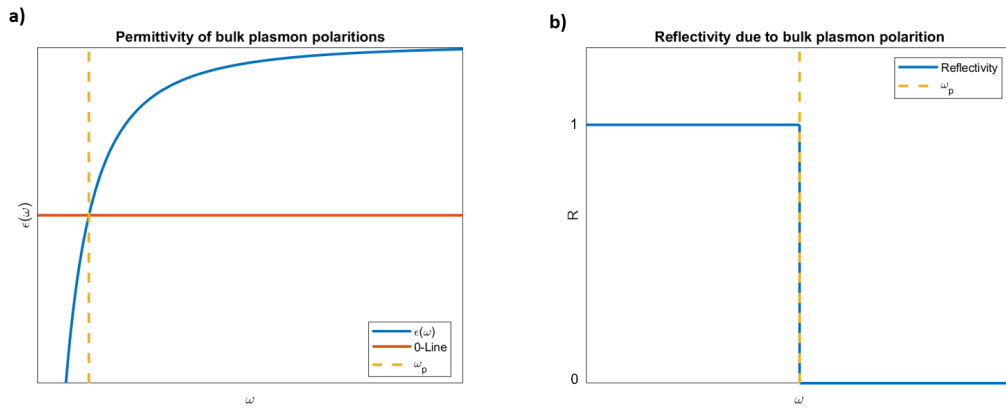


Figure 5: Graphical representation of plasma frequency properties. a) Plasma frequency in the real part of permittivity ϵ . It is easy to observe that $\epsilon(\omega_p) = 0$. b) Plasma frequency in a reflectivity plot. Here, it can be extracted that for $\omega = \omega_p$ a drop in reflectivity will be observed.

Dielectric function in reality In reality the Drude dielectric function is not always correct. Not only free electrons have to be considered but also interband transitions. This leads to a slightly different dielectric function than predicted from Drude's theory. Especially in the visible range this can easily be seen. In Figure ?? a comparison of experimental data and Drude model is shown.

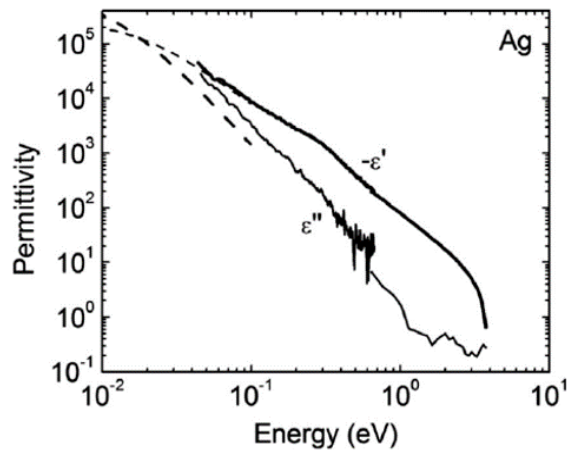


Figure 6: Real (ϵ') and imaginary (ϵ'') part as measured for silver (Ag). In dashed lines the Drude model dielectric function is indicated. A clear discrepancy is seeable mostly due to interband transitions. Grafic taken from [?].

2.3 Plasmon polaritons

In metals two major excitations are possible: plasmons and phonons. Plasmons are collective charge carrier oscillations. Phonons resemble collective lattice oscillations but will not play a role in this thesis. One major property of plasmons is their ability to couple with a photon resulting a coupled state called plasmon polariton. These states can be divided into three subcategories

1. Bulk plasmon polaritons
2. Surface plasmon polaritons
3. Particle plasmon polaritons

2.3.1 Bulk plasmon polaritons

In the following paragraph bulk plasmon polaritons (BPP) - material excitations due to a longitudinal oscillating plasma - will be discussed.

For the dispersion relation of BPP a transverse incident electromagnetic wave with wavevector \mathbf{k} and oscillation direction of electrical field \mathbf{E} perpendicular is assumed. Furthermore the important relation $k^2 = \epsilon\omega^2/c^2$ as already derived in equation ?? has

to be considered. Using this equation and the Drude dispersion relation for zero damping as derived in equation ?? one obtains the dispersion relation of bulk plasmon polaritons

$$\omega = \sqrt{\omega_p^2 + k^2 c^2} \quad (14)$$

It is easy to see that bulk plasmon polaritons are only possible for $\omega \geq \omega_p$. The dispersion relation is plotted in figure ??.

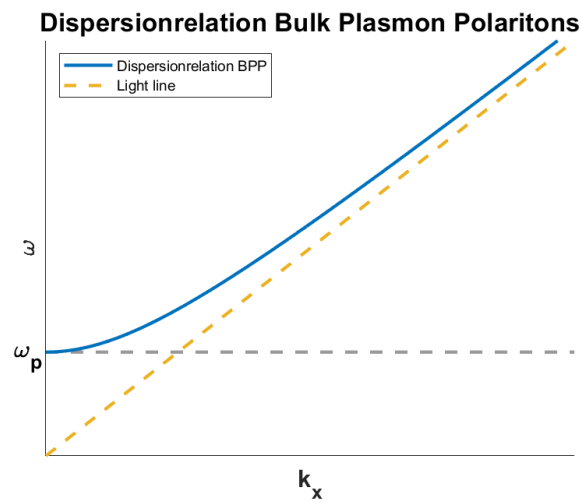


Figure 7: Dispersionrelation of bulk plasmon polaritons as plotted in blue. In yellow the light line is presented. Also the plasma frequency ω_p is indicated as a grey line. Note that only frequencies $\omega \geq \omega_p$ are allowed.

2.3.2 Surface plasmon polaritons

Surface plasmon polaritons (SPP) are electromagnetic excitations that propagate in a wave like fashion along a planar interface between a metal and a dielectric medium. Along the propagation distance the amplitude of the SPP decays exponentially. Its electromagnetic field is confined to the area very close to the surface resulting in enhancement of the electromagnetic near field.

To derive the dielectric function for surface plasmon polaritons one has to take into account a setup as demonstrated in figure ?? a). Here, the interface between a metal and a dielectric material is located at $z = 0$. For simplicity a SPP propagating in x -direction with wavevector k_x is assumed.

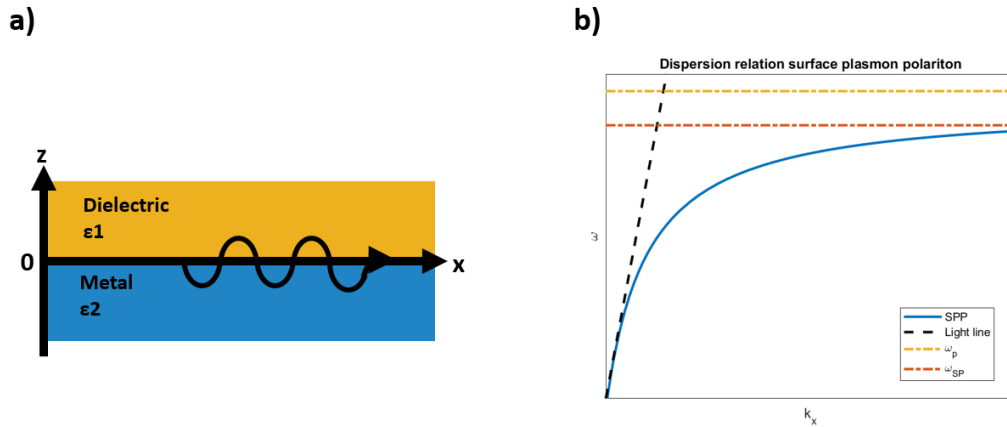


Figure 8: a) Schematic presentation of a two material (Dielectric and metal) interface in x - z -plane. The interface is located at $z = 0$. The sketched wave represents a charge density wave in the metal. b) Dispersion relation of SPPs (blue line). The light line ($\omega = ck_x$) is plotted in black. The red line corresponds to the high k limit of ω_{SP} . It can be noticed that other than for bulk plasmon polaritons the dispersion relation for SPPs is always smaller than the light line.

Using again the transverse electromagnetic wave approximation as well as the Maxwell conditions for a metal dielectric interface one can derive the following dispersion relation where ϵ_1 denotes the permittivity in the dielectric and ϵ_2 in metal.

$$\omega = \sqrt{\frac{\epsilon_2(\omega) + \epsilon_1}{\epsilon_2(\omega)\epsilon_1}} ck_x \quad (15)$$

This resulting dispersion relation for SPPs is plotted in figure ?? b).

2.3.3 Particle Plasmon Polaritons

Particle plasmon polaritons (PPP) are non-propagating excitations of the conduction of electrons in the conduction band in metallic nanostructures. Their behavior is strongly related to the boundary conditions given by the nanostructures dimensions and material as well as the surrounding medium. Particle plasmon polaritons are also called localized plasmon polaritons (LPP).

An exact theoretical description of particle plasmon polaritons is very difficult. Therefore long numerical simulations are required. However, for some symmetric particles such as spheres Mie theory [?] can be used to provide an exact solution. In 1912, Richard Gans further developed Mie theory for the description of spheroids [?]. Using Gans' theory an approximation of resonance behavior for nanoantennas can be made approximating them as elongated spheroids.

In Gans theory the electrical field component in x-direction E_x inside the spheroid with permittivity $\epsilon(\omega)$ surrounded by a medium of permittivity ϵ_d is defined as

$$E_x = \frac{1}{1 + \left(\frac{\epsilon(\omega)}{\epsilon_d} - 1\right)L} \cdot E_x^0 \quad (16)$$

At its resonance frequency the electrical field is the strongest. Therefore the following resonance condition as to be met

$$1 + \left(\frac{\epsilon(\omega)}{\epsilon_d} - 1\right) \cdot L = 0 \quad (17)$$

Again using the Drude dielectric function (equation ??) with zero damping one can derive the theoretical expected resonance frequency of a nanoantenna

$$\omega_{res} = \sqrt{\frac{\omega_p^2}{1 - (1 - L'^{-1})\epsilon_d}} \quad (18)$$

2. Theoretical Background

Here, L' is a factor depending on the dimensions of the antenna. For a antenna of length and width W , L' is defined as

$$L' = \frac{1 - e^2}{e^2} \cdot \left(\frac{1}{2e} \cdot \ln\left(\frac{1+e}{1-e}\right) - 1 \right) \quad (19)$$

Here, e is the ellipticity defined as $e^2 = 1 - (W/L)^2$. In figure ?? the theoretically expected behavior of nanoantennas for a length sweep from $2.5\mu\text{m}$ to $3.5\mu\text{m}$ is plotted. A width of $W = 100\text{nm}$ was assumed. A almost linear correlation was found between wavenumber and resonance position. For higher wavenumbers the resonance frequency decreases.

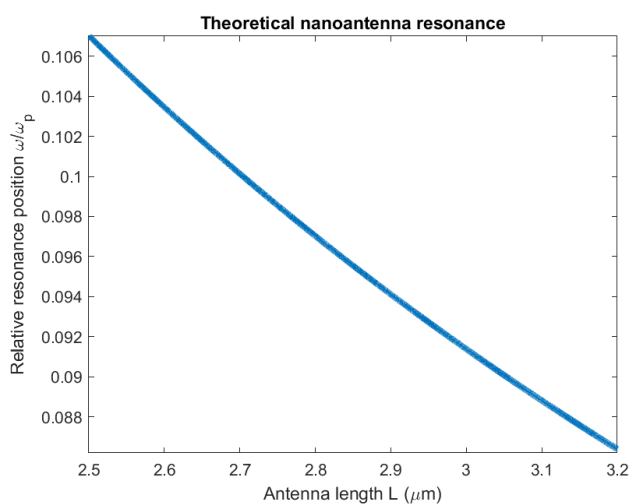


Figure 9: Theoretically calculated resonance position behavior of nanoantennas in a length sweep using Gans theory.

2.4 Nanoantennas

A nanoantenna, as it will often be referred to in the following, is a cylinder of a well defined length L , height H , width W and material. The length is in a range of a few hundred nanometers to a few micrometers. For the following an electrical field oscillating parallel to the long axis of the nanorods will be assumed. A plasmonic resonance in direction perpendicular to the long nanorod axis is also observable but much weaker and thus not suited for surface enhanced infrared spectroscopy even though it can be used for reference measurements.

2.4.1 Single nanoantennas

In the following paragraph some properties of single isolated nanoantennas will be discussed.

Resonance For an antenna of length L in the surrounding medium of refractive index n the resonance wavelength λ_{res} of mode number m is given by

$$\lambda_{res} = \frac{2L}{m} n a_1 + a_2 \quad (20)$$

Here, a_1 denotes a constant corresponding to the phase of the reflection at the antenna end, a_2 is a geometry and material constant. Both constants gain importance for smaller antennas especially with resonances in the infrared region.

From above equation one can extract an important relation for the first mode ($m = 1$)

$$\omega_{res} \propto L^{-1} \quad (21)$$

Evaluating equation ?? one expects a δ -formed antenna resonance. In reality one observes a broadening of this resonance due to the damping caused by collisions of electrons with ionic cores. When measuring with darkfield microscopy the remainder radiation has also a broadening effect.

2. Theoretical Background

E-field enhancement As explained before in nanotennas electrical near fields are strongly enhanced due to plasmonic resonances. Near-fied enhancement for a single gold nanoantenna of length $L = 400\text{nm}$ and width $W = 80\text{nm}$ is shown in figure ?? a). Note that the enhancement is especially strong at both ends of the nanoantenna. This effect is called lightning rod effect [?]. Since a high electrical field is needed for infrared absorption, as it will be discussed in the following, nanoantennas are perfectly suited for surface enhanced infrared spectroscopy.

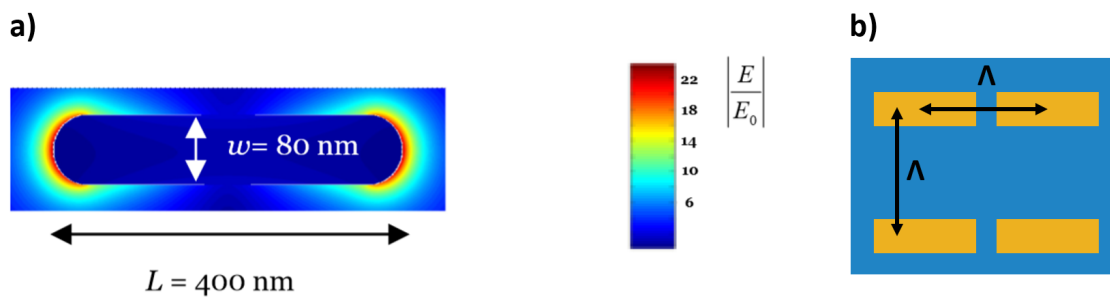


Figure 10: a) Enhancement of electrical field E by a single nanoantenna with round edges of given dimension as indicated in the picture. The strength of enhancement is given by the color bar on the right. Graphic taken from [?]. b) Sketch of periodically arranged nanoantennas (gold) on glass substrate (blue) with periodicity Λ .

2.4.2 Interaction of periodically arranged nanoantennas

In this thesis the nanoantennas will be arranged periodically on a substrate giving rise to a few properties. The defining factor for the mesh the antennas are arranged in is the periodicity Λ . Since in this thesis in x- and y-direction periodicity will always be the same it is suited to consider only one parameter. This parameter defines the distance from the short side middle of one antenna to the short side middle of another antenna and at the same time the long side middle of one antenna to the long side middle of another. A sketch is shown in figure ?? b).

Resonance In periodically arranged nanostructures near-fields are additionally enhanced compared to single nanoparticles. This enhancement is due to the interaction of scattered far- and near-fields of the antennas (for a separation larger than 100 nm) and occurs if below condition (see equation ??) is fulfilled. For the resonance frequency the following relation is given

$$n_s \cdot \omega_{\text{collective}} \approx \sqrt{\left(\frac{i}{\Lambda_x}\right)^2 + \left(\frac{j}{\Lambda_y}\right)^2} \quad (22)$$

Here, n_s denotes the refractive index of the substrate, $\omega_{\text{collective}}$ is the resonance wavenumber of the lattice mode (in cm^{-1}), i and j represent the order of excitation parallel and perpendicular to the long antenna axis and Λ_m is the periodicity in direction m . In this thesis constant periodicity in all directions is used ($\Lambda_x = \Lambda_y = \Lambda$) and only the first order of diffraction parallel to the long antenna axis is of interest ($i = 1, j = 0$) which deduces

$$\Lambda \approx \frac{1}{n_s \cdot \omega_{\text{collective}}} \quad (23)$$

Spectral response The spectral response of periodically arranged nanoantennas is slightly different than of a single nanoantenna. Two resonances - one by the antenna and one by the periodic arrangement (in this thesis called 'mesh resonance') - occur. In figure ?? a) such a spectral response of gold nanoantennas with $L = 3.244\mu\text{m}$, $H = W = 100\text{nm}$ and $\Lambda = 5.76\mu\text{m}$ is shown. The antenna resonance is highlighted in

2. Theoretical Background

red and was determined in the following as the minimum of a Lorentzian fit to the the antenna resonance area. The mesh resonance is highlighted in blue and was determined as the highest point of the spectral area around. Both resonances can be described by a harmonic oscillator approximation. In nanoantenna arrays these two harmonic oscillators couple to each other resulting in a coupled oscillator. In figure ?? b) the near-field enhancement of a isolated and a periodically arranged antenna are compared. The signal of periodically arranged antennas is roughly 4 times stronger than of a isolated antennas.

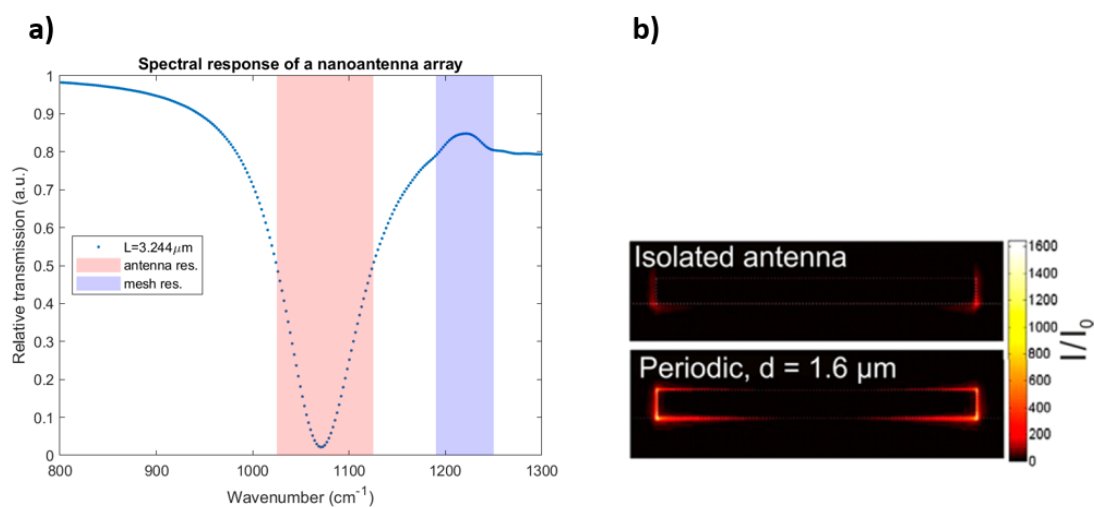


Figure 11: Spectral response of periodically arranged gold nanoantennas. a) spectral response of a gold nanoantenna array of length $L = 3.244\mu\text{m}$. b) Numerically calculated distribution of near-field intensity for a single antenna and a periodically arranged antenna array. Graphic for b) taken from [?].

2.5 Infrared spectroscopy

Infrared spectroscopy is a commonly used technique in science and industry. It is based on the interaction of infrared electromagnetic radiation and matter which can be in the state of a solid, liquid or gas.

When a sample is radiated with light a excitation of molecular binding is provoked as well as molecular rotations. This occurs at certain frequencies - resonate frequencies ω_{vib} . For infrared spectroscopy the sample has to be 'infrared-active', meaning that it has to feature a time depended electrical dipole moment.

Description of infrared spectroscopy with harmonic oscillator Molecules when penetrated with infrared light can be described as harmonic oscillators. Force constants are given by their type of binding. The bonds can be excited into different oszillation modes. This leads to different energy levels with constant energy displacement. When IR light is shined on a sample, modes are excited into higher ones resulting in a decreased transmission of the incident light and at the same time in increased extinction. Since different atomic groups as well as different atomic binding produce different signals infrared spectroscopy is a good tool for substance identification.

Infrared absorption For the absorption A of IR light by molecules the following relation is given

$$A \propto |E_{\text{local}}|^2 \quad (24)$$

This induces that strong electrical near-fields are required for a good infrared spectroscopy signal.

2.5.1 SEIRA

In this section surface enhanced IR absorption (SEIRA) will be discussed. In this thesis nanoantenna arrays were selected for enhancement. When being penetrated with light plasmonic resonances are provoked resulting in a strongly decreased relative transmis-

2. Theoretical Background

sion and increased extinction around the resonance frequency. When measuring vibrational bands of other materials the strongest signal enhancement can be produced for a match of plasmonic and vibrational resonance.

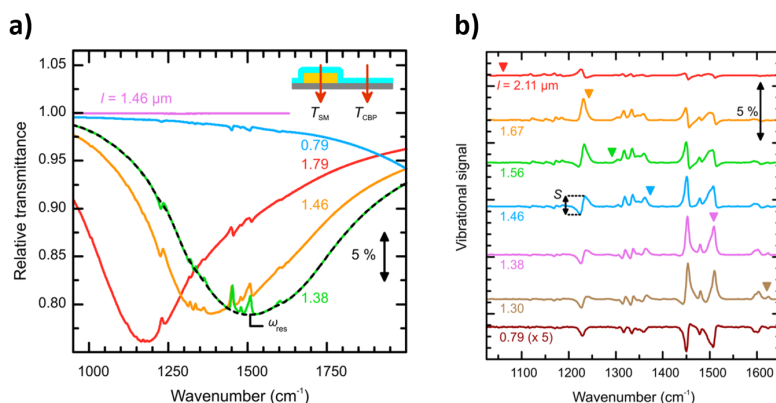


Figure 12: Signal enhancement by surface enhanced infrared absorption (SEIRA). a) Relative transmittance as measured for selected antenna arrays of different length as indicated in the legend. The measurements were performed with a 4,4'-bis(Ncarbazolyl)-1,1'-biphenyl (CBP) coated antenna resulting in an enhancement of its vibrational signal. This can be seen as derivation from the Lorentzian shape of transmittance spectra. Graphic taken from [?]. b) Baseline corrected spectra of selected nanoantennas of varying length. The plasmonic resonance is indicated by the triangles. Graphic taken from [?].

In figure ?? a) results of a SEIRA measurement are shown. Nanoantenna arrays of selected length coated with CBP were analyzed. A clear derivation of the signal from a Lorentzian shape can be seen due to the coupling of plasmonic resonance and vibrational resonance of CBP. The derivation is especially strong for $l = 1.38\mu\text{m}$ (green curve) but also in all other curves the vibrational mode of CBP at around 1475cm^{-1} is visible. For a length of $l = 1.38\mu\text{m}$ the condition $\omega_{vib} = \omega_{plasmon}$ is fulfilled resulting in a especially strong signal enhancement. In figure ?? b) baseline corrected relative transmittance spectra of selected nanoantenna arrays are shown. The plasmonic resonance is indicated with a triangle. Here, as in a) strong signal enhancement can be detected for good match of vibrational resonance and plasmonic resonance.

3 Methods

This Chapter will focus on the used methods for data acquisition. First the simulation software 'Lumerical FDTD Solutions' will be presented. The simulation setup as well as the simulation method and a mesh convergence measurement will be discussed. In the last part Fourier transform infrared spectroscopy as used for measurements during this thesis will be presented.

3.1 Lumerical FDTD Solutions

3.1.1 Simulation setup

Lumerical FDTD Solutions is a simulation software specially designed for condensed matter applications. It is used for solar cell simulations over OLED to surface plasmon simulations.

Concept Lumerical FDTD Solutions uses the finite-difference time-domain (FDTD) method, commonly used in modeling computational electrodynamics. It works by discretizing the animated structure into subcells solving the time-dependent Maxwell's equations in partial differential form using approximations. The accuracy as well as the position of the mesh can be selected when designing a structure.

Environment Lumerical FDTD Solutions offers a 3D CAD platform for design and variation of the desired setup. It includes a list of all used structures and materials as well as a separate window for all simulation results. The integrated script editor is another important feature for acclimatization of tasks.

Setup for simulations The simulation setup consists of the following elements:

Source As a source the preinstalled Lumerical 'Total field scattered field' source was selected. It features the splitting of the resulting total field (sum of incident field and scattered field) and the scattered field. The incident wave is a plane wave with prese-

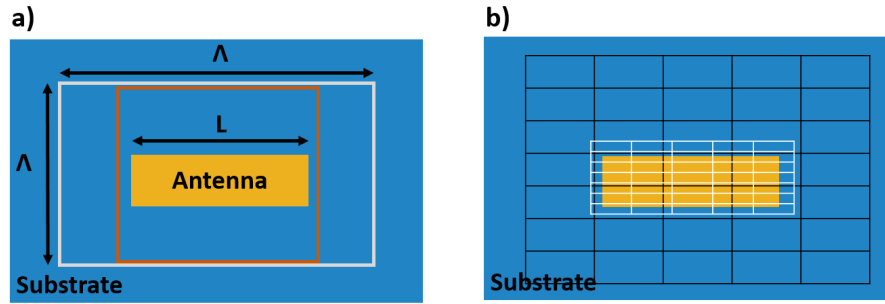


Figure 13: Schematic representation of simulation setup. a) Topview of simulation setup. In blue the substrate is shown. The grey box represents the simulation region which defines the periodicity Λ . In red the region of field measurement is represented. The electromagnetic source is located inside of the substrate with its origin in the middle of the antenna. Its propagation direction is out of the observation plane. b) Topview on antenna (yellow) with mesh (black) and submesh (white).

lected oscillation direction of the electrical field.

Mesh The mesh size in combination with the chosen boundary conditions defines at how many points Maxwells equations are solved and therefore how accurate the data represent the reality. Its size also defines the setup of the infinitely large array that is being simulated if boundary conditions are chosen that way. As boundary conditions antisymmetric in x direction, symmetric in y direction and perfectly matching layer in z direction were chosen (see ??).

Submesh The submesh encloses with a little offset the nanoantenna and gives extra mesh points for the software to analyze. To determine its accuracy a convergence measurement was done.

Substrate For a substrate glass was chosen to produce data that is comparable to measurements. Therefore a reflective index of $n = 1.41$ for the substrate was selected.

Antenna The antenna is the main part of the simulation. Its length and width as well as the material determine together with the mesh dimension the spectral response of the structure. These parameters are alternated in the course of this thesis. Also for each measurement a reference without an antenna was taken which will be discussed later.

Analysis boxes Analysis boxes are another relevant part of this simulation. In figure ?? they are shown in red. Each box contains a number of monitors. For further calcula-

tions only the upper layers in z-direction of each box are considered. Here the output power was measured and thus the relative transmission calculated.

Direction	Boundary condition	Explanation
x-direction	antisymmetric	enables E-field perpendicular to the border
y-direction	symmetric	enables E-field parallel to the border
z-direction	perfectly matched layer (PML)	absorbs electric and magnetic field reflectionless

Table 2: Boundary conditions as used for all FDTD simulations in Lumerical FDTD Solutions

Boundary Conditions In general boundary conditions are designed to reduce calculation time by setting unused field components to zero. They have to be carefully selected to fit the setup symmetry as well as the source symmetry. The boundary conditions in the simulations carried out during this thesis (see table below) have been selected to fit the incident light. It has an electric field oscillating in x-direction. As mentioned before a electrical field component parallel to the long axis of the nanorod is critical to ensure the desired resonant behavior.

In x-direction antisymmetric boundary conditions were selected to ensure that the electrical field is reflected back onto the long axis of the nanoantenna. In real measurements the same takes place through reflection of electrical field from other nanoantennas.

To make sure no electrical field escapes the simulation region on the long sides of the antenna a symmetric boundary condition in y-direction was selected. It only allows a electrical field parallel to the boundary and absorbs the E-field perpendicular to it.

For simulation of an open boundary a perfectly matched layer boundary (PML) was chosen in z-direction. It absorbs reflectionless all light incident upon it. This way it also ensures that all incident light only passes through the antenna once.

3.1.2 Simulation method

In this section the measurement method of all simulations will be explained. A graphical representation of it is shown in figure ??

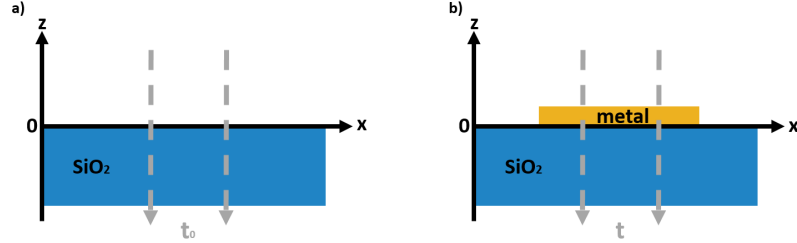


Figure 14: Graphical representation of measurement method. The substrate (blue) structure interface is located at $z = 0$. A cut in the x - z -plane is shown. a) Measurement of transmitted light without structure on top of substrate. b) Measurement of transmitted light with metal structure on top of substrate.

For all simulations relative transmittance t_{rel} was extracted measuring transmittance without a structure on the substrate t_0 and the transmittance with a structure on top of the substrate t . The following relation was used to then calculate relative transmittance.

$$t_{rel} = \frac{t}{t_0} \quad (25)$$

Due to the fact that $t_0 > t$ and $t_0 > 0$, $t > 0$ the relative transmittance is expected to fulfill $0 < t_{rel} \leq 1$

3.1.3 Mesh convergence

In this section the optimization as it was done for the submesh will be described. Simulation time is strongly depended on mesh accuracy. Therefore a submesh located around the nanoantenna (x -span = $7\mu\text{m}$, y -span = $0.2\mu\text{m}$, z -span = $0.2\mu\text{m}$) was introduced. Optimization of submesh accuracy in terms of calculation time is a point of interest. Therefore the same setup (gold antenna, $L = 1.7\mu\text{m}$, $H = 0.1\mu\text{m}$, $W = 0.1\mu\text{m}$) was simulated for different submesh settings. The results are shown in figure ??.

As it can be seen in figure ?? for a submesh gratings bigger than 15nm extrema ap-

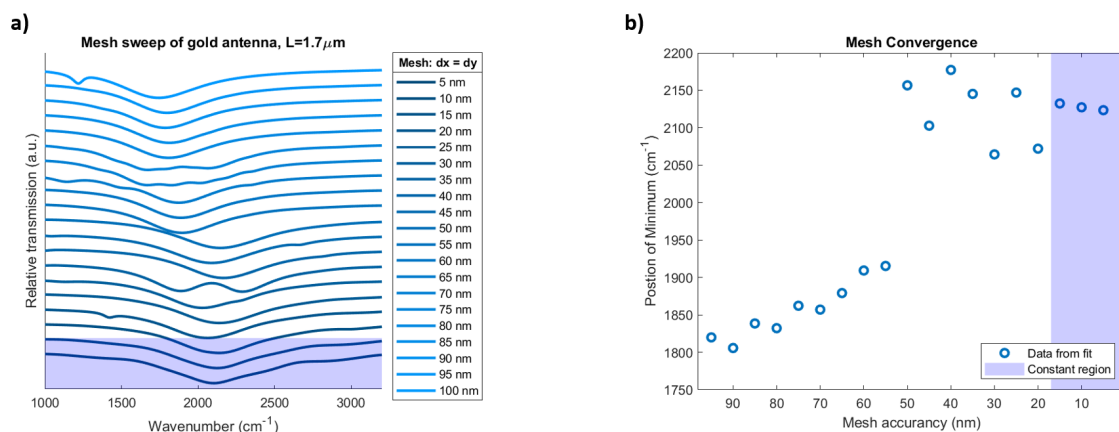


Figure 15: Results of FDTD Simulation with different submesh accuracy. a) Spectral response of nanoantenna of length $L = 1.7\mu\text{m}$ with array periodicity chosen so that almost no coupling of array and antenna resonance occurs. The submesh grating is indicated by $dx = dy$ and varied from 100nm to 5nm. The constant region as found in b) is highlighted in blue. b) Position of antenna resonance versus mesh grating. Antenna resonance position was determined by a Lorentzian fits.

pear that vanish with increasing submesh accuracy. For example the dip at around 1210cm^{-1} disappears for an increase in mesh accuracy of 5nm to 95 nm already. Due to these results a submesh grating of 15 nm was chosen for all further simulations of one material nanoantennas.

3.2 Fourier transform infrared spectroscopy

In this paragraph the general working principle of Fourier transform infrared spectroscopy (FTIR) will be discussed. The main part of an infrared Fourier spectrometer is its Michelson interferometer that is used for analysis for the incident light. After passing through the probe the IR light is directed into the interferometer where it is divided by a beam splitter into two beams. One of them is directed onto a mirror of fixed position and reflected back. The other one encounters a movable mirror inducing an optical path difference Δx . After reflection both beams come together again and interfere.

Assuming monochromatic IR light the intensity I at the detector position depending on path difference Δx and wavenumber ω is given by

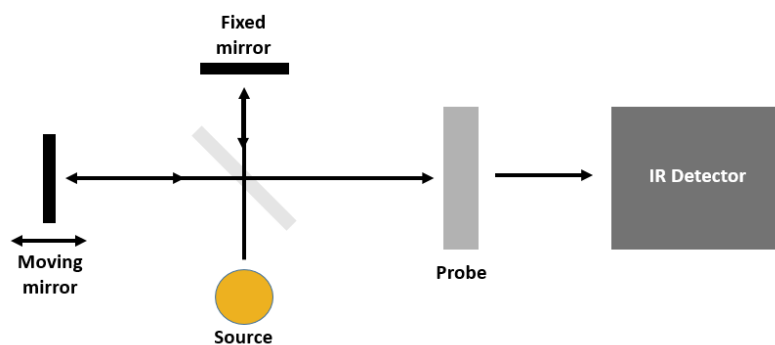


Figure 16: Schematic representation of Fourier transform infrared spectroscopy working principle.

$$I(\Delta x, \omega) = I_0(\omega) \cdot (1 + \cos(\omega \Delta x)) \quad (26)$$

For polychromatic light as used in FTIR an integration over all wavenumbers has to be performed

$$I(\Delta x, \omega) = \text{const} + \int_0^{\infty} I_0(\omega) \cdot \cos(\omega \Delta x) d\omega \quad (27)$$

Taking the Fourier transform of above equation one can transfer the spectral information into frequency space and ends up with a frequency spectrum as desired.

4 Results

In this chapter the obtained results are presented. Enhancement effects of nanoantennas will be analyzed. After that simulations done for tuning of resonances as well as the optimization results will be presented. In the following multilayer system simulations for gold coated on aluminum, gold coated on copper and gold coated on magnesium will be analyzed. A gold cap length sweep was done on copper, aluminum and magnesium antennas. In the last part Fourier transform infrared spectroscopy measurements of gold coated aluminum nanoantennas with and without HMDS coated onto the substrate will be presented and analyzed.

For all simulations conducted, antenna arrays of periodicity Λ , height H , width W and length L were used. All parameters are shown in figure ??.

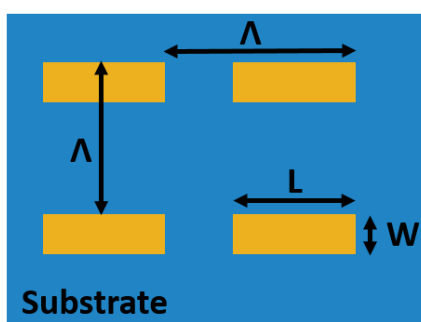


Figure 17: Setup for simulations conducted. The x-y-plane is shown.

4.1 Enhancement of E-field by nanoantennas

In figure ?? electrical field enhancement $|E/E_0|$ at different antenna positions in a resonant gold nanoantenna is shown. The substrate can be seen in a) and b) as a light blue rectangle on the bottom of the picture.

Electrical near-field enhancement is very strong within a few tenth of nanometers around both ends of the antenna. Especially at the antenna edge it is strongly enforced as expected from theory. The enhancement factor is around 250.

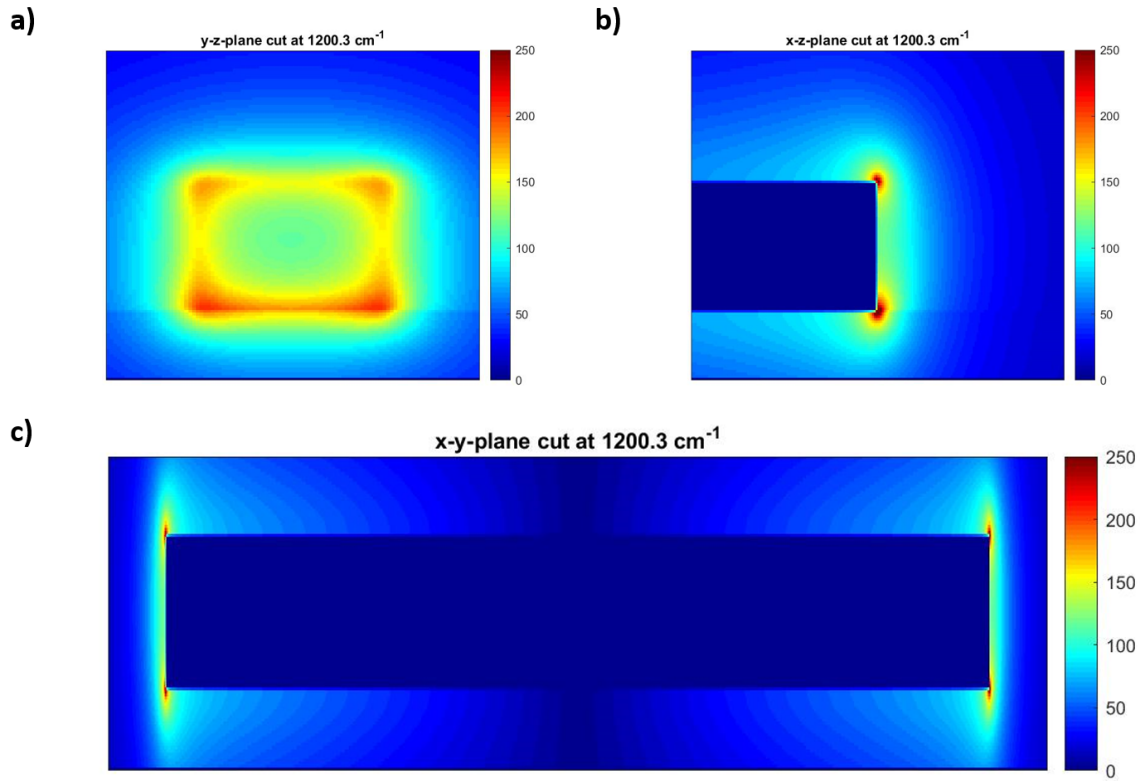


Figure 18: Enhancement of electrical field in and around resonant gold nanoantenna of dimensions height $H = 100\text{nm}$, width $W = 100\text{nm}$, length $L = 2.84\mu\text{m}$ and periodicity $\Lambda = 5.22\mu\text{m}$. The antenna is located in the x-y-plane its long side in x-direction. The absolute value of electrical field enhancement $|E/E_0|$ is given as indicated by the colorbar. a) Cut in y-z plane at position $x = L/2$ (short end of antenna) b) Cut in x-z-plane at position $y = 0\text{nm}$ (half antenna width) c) Cut in x-y-plane at position $z = 50\text{nm}$ (half antenna height).

4.2 Tuning of resonances for SEIRA

4.2.1 Antenna length sweep

In this section the general relation of nanoantenna length and plasmonic resonance will be analyzed. Therefore, a length sweep in steps of $0.1\mu\text{m}$ was performed while keeping all other parameters such as periodicity Λ , height H and width W constant. The results of a gold antenna length sweep are shown in figure ??.

As predicted from theory two resonances are clearly visible for each combination of antenna length L and periodicity Λ (see figure ?? a). The red highlighted plasmonic

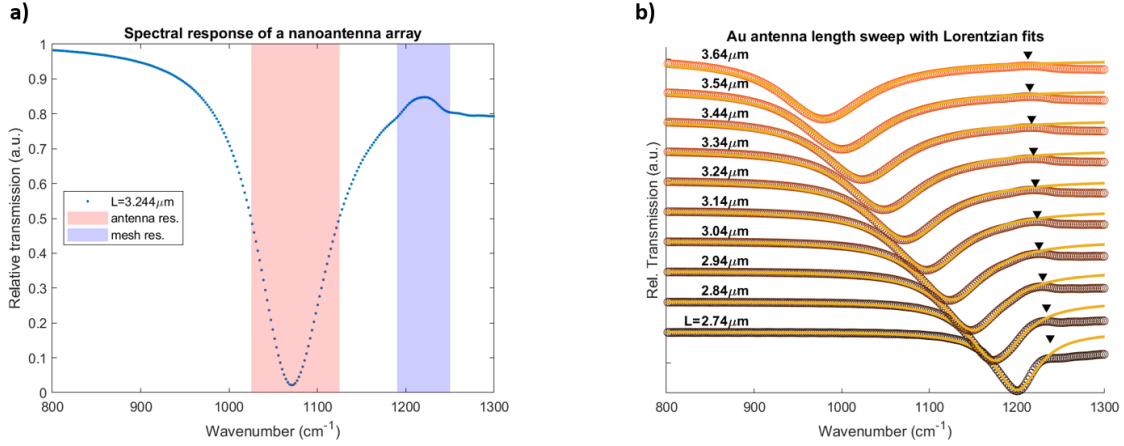


Figure 19: Results of FDTD simulation of gold nanoantennas. Their dimensions are given as $W = 0.1\mu\text{m}$ and $H = 0.1\mu\text{m}$. Length L is varied in $0.1\mu\text{m}$ steps from $2.744\mu\text{m}$ to $3.744\mu\text{m}$. For periodicity $\Lambda = 5.758\mu\text{m}$ was chosen. a) Spectral response of one nanoantenna array of length $L = 3.244\mu\text{m}$. The plasmonic resonance is highlighted in red, the resonance due to periodically arrangement is blue highlighted. b) Antenna length sweep from $L = 2.74\mu\text{m}$ to $L = 3.64\mu\text{m}$ as indicated by the legend on the left. In yellow Lorentzian fits for the antenna resonances are shown. Triangles indicate the mesh mode.

resonance (in the following also called antenna resonance) corresponds to the dip at 1074.9cm^{-1} . A Lorentzian fit was performed. The plasmonic resonance was determined as the wavenumber of minimum transmission. The resonance from periodically arrangement (in the following also called mesh resonance) is highlighted in blue. It was determined as the maximum transmission to a value of 1220.9cm^{-1} . As described in section ?? both resonances are coupled. In figure ?? b) the obtained spectra of an antenna length sweep are shown. Gold nanoantennas were simulated. As expected from theory plasmonic resonance is length dependent. With increasing length the resonance shifts to lower wavenumbers. Comparing this result to the prediction from Gans theory (see figure ??) this is just as expected. The exact relation will be discussed in the following paragraph. Also a good agreement of antenna resonance and Lorentzian fit can be noticed.

In figure ?? b) the position of mesh mode is plotted as black triangles. Mesh resonance is almost constant for all antenna lengths. This is due to the constant periodicity of $\Lambda = 5.758\mu\text{m}$. The variation that is detectable is due to coupling of antenna and mesh mode as described in section ?? which gets stronger the closer the antenna resonance approaches the mesh resonance.

4.2.2 Analysis of antenna resonance in a antenna length sweep

In figure ?? b) a relation between antenna resonance and antenna length can clearly be detected. With increasing antenna length L the antenna resonance is shifted to lower wavenumbers. Also a coupling between antenna resonance and mesh resonance can be seen as small shifts in mesh resonance. Despite this coupling the relation as derived for single antennas (see equation ??)

$$\omega_{\text{res}} \propto L^{-1} \quad (28)$$

should be analyzed here. Therefore, antenna resonance, determined using the Lorentzian fits, was plotted against corresponding length L . The results are shown in figure ?? a). Fit errors are also featured.

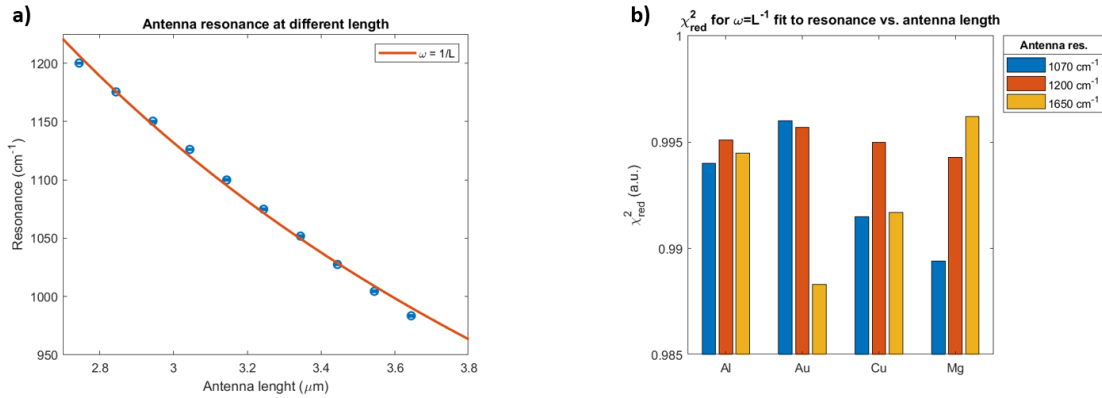


Figure 20: Dependence of antenna resonance to antenna length. a) Antenna resonance in dependence of antenna length for gold. The shown data points (blue circles) are extracted from Lorentzian fits. Fit errors are featured. Also, a fit was performed and is shown in red. b) Analysis of goodness of fit to antenna resonance in dependence of antenna length. Shown are the reduced χ^2 values for different elements and different spectral positions as indicated by the legend.

As predicted from theory in figure ?? a) a $1/L$ dependence between antenna length and antenna resonance was found. A fit was performed taking errors into account. For further analysis goodness of fit was inspected using the reduced χ^2 method. Results for all 4 materials are shown in figure ?? b). Obtained χ^2 values differ only in order of 10^{-2} from the optimal value of $\chi^2 = 1$. Thus, a very good agreement of $1/L$ dependence of antenna length versus resonance can be verified. The derivation from $1/L$ dependence

can be retraced to the interaction between antenna and mesh mode. Comparing figure ?? to the behavior as expected from Gans theory (see figure ??) strong similarities can be found.

4.2.3 Optimization results

To optimize the nanoantenna arrays for the desired application in surfaced enhanced infrared spectroscopy (see section ??) it was required to select periodicity Λ and length L such that the antenna resonance is according to the vibrational mode of the selected materials. In table ?? these wavenumbers are shown. A offset between antenna and mesh resonance of 150cm^{-1} was selected to keep coupling effects small.

$\omega_{vib}(\text{cm}^{-1})$	$\omega_{mesh}(\text{cm}^{-1})$	For Analysis of
1070	1220	DNA
1200	1350	HMDS
1650	1800	Protein Amide I group

Table 3: Vibrational modes of materials to be measured. Periodicity Λ and antenna length L have to be selected so that $\omega_{vib} = \omega_{antenna}$. Antenna resonance is similar to plasmonic resonance. The corresponding materials are also shown. The mesh resonance was selected to be $\omega_{mesh} = \omega_{vib} + 150\text{cm}^{-1}$.

For tuning of antenna and mesh mode to the desired wavenumbers as shown in table ?? iterative testing was done. As starting parameters predictions from equation ?? and ?? were used. Both resonances were optimized to a precision of $\pm 6\text{cm}^{-1}$. All results are shown in table ??.

4.2.4 Comparison of expected periodicity to simulation

Using equation ?? and the known reflective index of the glass substrate $n_{subst} = 1.41$ the expected periodicity Λ_{theo} for each mesh mode can be calculated. Comparing these to the results as shown in table ?? it becomes clear that these must differ from the ones obtained in simulations. Theory predicts Λ to be the same for all materials which is clearly not the case. This might be due to lack of material constants taken into account for the derivation of formula ?. A comparison of theoretically expected and simulated periodicity Λ is shown in table ??

4. Results

	ω_{plasmon}	ω_{mesh}	L	Λ
Au	1074.88	1220.94	3.24	5.76
	1200.35	1351.76	2.84	5.22
	1647.76	1798.82	2.00	3.92
Al	1075.65	1218.82	3.36	5.78
	1200.78	1351.76	2.95	5.22
	1645.07	1800.71	2.09	3.92
Cu	1075.20	1220.94	3.17	5.75
	1201.69	1348.00	2.78	5.22
	1649.62	1800.71	1.94	3.92
Mg	1073.08	1220.94	3.19	5.83
	1200.04	1349.88	2.82	5.26
	1648.92	1800.71	1.99	3.93

Table 4: Summary of all optimized parameters as obtained for Au, Al, Mg, Cu. Note, that all shown frequencies ω are in cm^{-1} . Length L and Periodicity Λ are given in μm .

ω_{vib}	Λ_{theo}	Λ_{Au}	Λ_{Al}	Λ_{Cu}	Λ_{Mg}
1070	5.81	5.76	5.78	5.75	5.83
1200	5.25	5.22	5.22	5.22	5.26
1650	3.94	3.92	3.92	3.92	3.93

Table 5: Comparison of theoretically experted periodictiy Λ_{theo} as calculated using equation ?? and simulated periodictiy. Note that all frequencies ω are in cm^{-1} . All periodicities Λ are in μm

As shown in table ?? the derivation of periodicity as calculated using equation ?? and periodicity as resulted from simulations Λ is in order of $10^{-2}\mu\text{m}$. This corresponds to a derivation of 1σ for all materials and wavenumbers. Thus, the derivation is not significant. Therefore, the found coupling of plasmonic resonance and resonance from periodically arrangement for an offset of these two resonances of 150cm^{-1} is very small. Thus, antenna resonance and mesh resonance can be treated as almost independent. This result is according to the one found in section ?? for the antenna length antenna resonance dependence.

4.3 Multilayer systems

In this section simulations of multilayer systems, more precisely gold (Au) on top of aluminum (Al), gold on top of copper (Cu) and gold on top of magnesium (Mg), will be presented and analyzed.

4.3.1 Setup

For all simulations the optimized values of length L and periodicity Λ of Al, Cu and Mg for a plasmonic resonance of 1200cm^{-1} (see table ??) were selected. On top of the antenna an Au layer of thickness T was added. In the following a thickness sweep from 0nm to 100nm in steps of 10nm was performed. The remaining setup as discussed in section ?? stayed unchanged. A submesh grating of 5nm was chosen. A sketch of the setup is shown in figure ??.

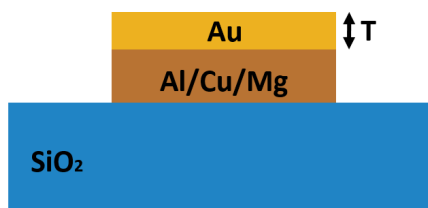


Figure 21: Side view of simulation setup for multilayer simulation. On top of a substrate (blue) a nanoantenna (brown) is located. On top of the antenna a gold layer (yellow) of thickness T is added.

Similar to prior simulations relative transmittance was measured. The source was located inside the substrate with radiation direction along the z -axis. The electrical field was polarized in the direction parallel to the antenna.

4.3.2 Au on Al

In the following paragraph simulation results of gold coated aluminum antennas in a gold thickness sweep will be discussed.

In figure ?? the spectral response of a thickness sweep of gold coated aluminum antennas is shown. Both resonances are clearly visible. In a) both the antenna and the mesh

4. Results

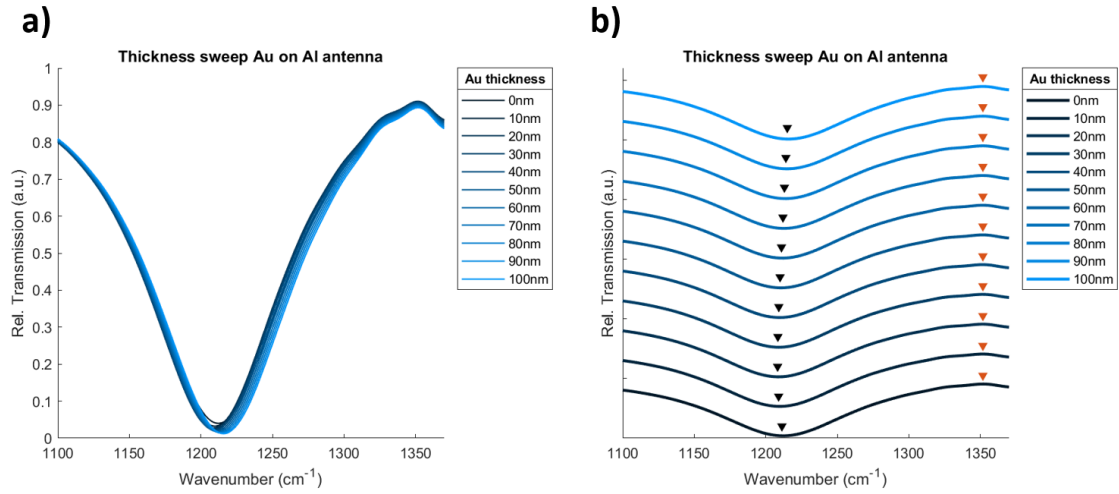


Figure 22: Simulation results of aluminum nanoantennas coated with a gold film of thickness as indicated by the legend. a) Typical spectral response due to thickness sweep. b) Spectral response with offset. The black triangles correspond to the antenna resonance as extracted from Lorentzian fits. The red triangles correspond to the mesh resonance.

resonance are almost constant. In b) a small shift in antenna resonance first to lower then to higher wavenumbers can be detected while the mesh resonance stays constant for all gold film thicknesses. Extinction is high for all aluminum antennas and stays almost constant through out all gold thicknesses.

For gold coated aluminum antennas spectral response is almost constant for all gold film thicknesses.

4.3.3 Au on Cu

In the following paragraph simulation results of gold coated copper antennas in a gold thickness sweep will be discussed.

In figure ?? the spectral response of gold coated copper antennas is shown. A shift in antenna resonance to higher wavenumbers can be found for increasing thickness T . Mesh resonance stays constant. Also a high extinction can be detected since T_{\min} is very low for all spectra.

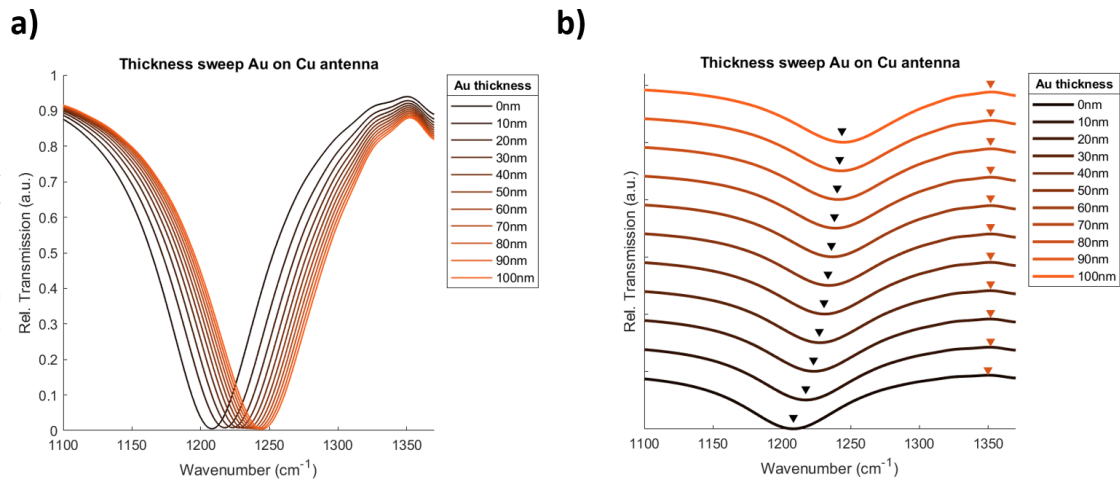


Figure 23: Simulation results of copper nanoantennas coated with gold films of thickness as indicated by the legend. Figure setup similar to figure ??.

4.3.4 Au on Mg

Here, the influence of a gold film with varying thickness T on top of a magnesium antenna will be discussed and analyzed.

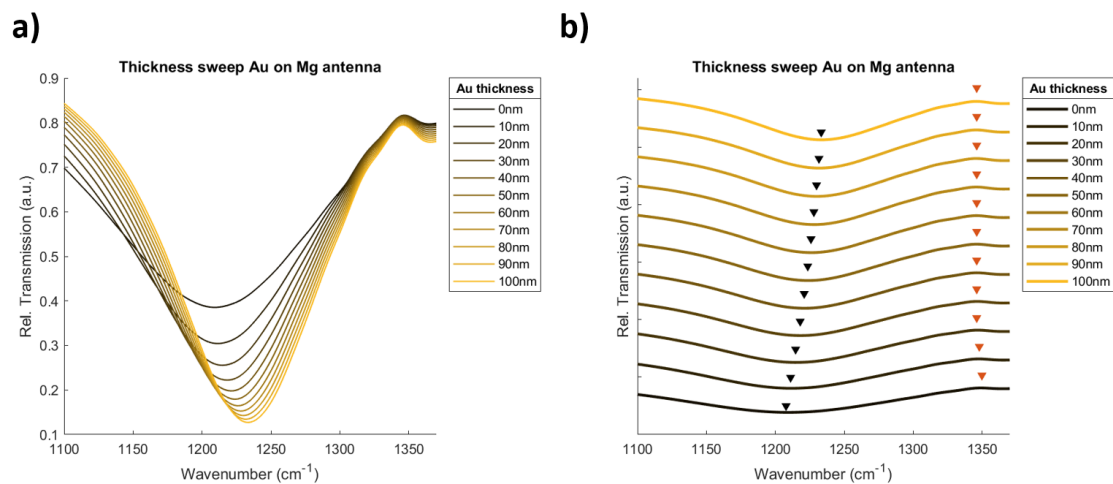


Figure 24: Simulation results of magnesium nanoantennas coated with a gold film of thickness as indicated by the legend. Figure setup similar to figure ??.

In figure ?? the spectral response due to a thickness sweep for a gold coated magnesium antenna is shown. Plasmonic resonance is shifted to higher wavenumbers for increas-

4. Results

ing thickness. Mesh resonance is constant. Also a signal enhancing behavior of gold can be seen, since minimal transmission T_{min} decreases for increasing gold thickness. Thus, extinction increases.

For all materials a constant resonance of periodically arrangement was detected. This is due to the constant periodicity and the before done tuning of antennas so that antenna and mesh mode can be treated as almost isolated.

4.3.5 Analysis of antenna resonance and extinction for all three materials

In this section the antenna resonance behavior during a gold layer thickness sweep will be further analyzed and compared for aluminum, copper and magnesium antennas.

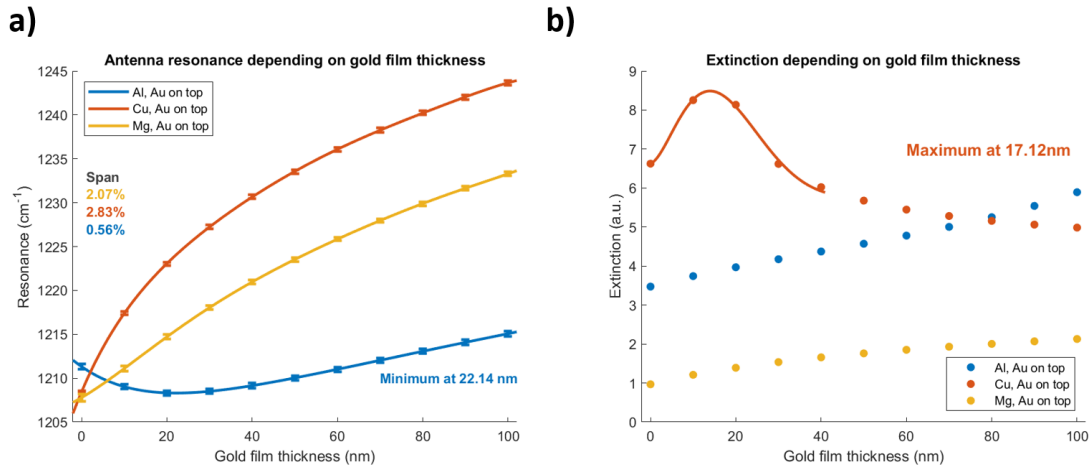


Figure 25: Analysis of gold layer thickness sweep for all three antenna materials. a) Antenna resonance position in dependence of gold film thickness T . b) Maximum extinction.

In figure ?? a) plasmonic resonance is plotted against gold film thickness for aluminum, copper and magnesium antennas. To determine the minimum position of the aluminum antenna resonance an polynomial fit was done which is features as well as the minimum position of the aluminum curve. The featured errors correspond to the fit errors. For all three curves a shift of resonance to higher wavenumbers was found for increasing gold film thickness. Surprisingly antenna resonance for aluminum antennas slightly decreases to a minimum at 22.14nm before starting to increase again.

Compared to their resonance position the total shift from $T = 0\text{nm}$ to $T = 100\text{nm}$ of antenna resonance is small. It is featured in the figure ?? a). For copper and magnesium the maximum shift is at about 2% of their resonance position with $T = 0\text{nm}$, for aluminium only 0.6%.

In multilayer systems, as simulated here, total spectral response is almost similar to nanoantennas of only one material and increased thickness. Since both materials are conductors and the plasmonic resonance is due to oscillating charge carrier electrons can be exchanged. Thus, the antenna acts as if made from only one material. In equation ?? this leads to a changed geometry and material constant a_2 (height H is increased) resulting in a changed expected plasmonic resonance depending on the gold film thickness. This explains the shift in antenna resonance when gold film thickness is varied. Additionally boundary conditions of the interface for both materials are changed. This as well has an effect on the plasmonic resonance.

In figure ?? b) maximum extinction in dependence of gold film thickness was plotted for all three materials. Maximum extinction E was calculated using

$$E = \ln\left(\frac{1}{T(\omega_{\text{plasmon}})}\right) \quad (29)$$

With increasing gold layer thickness extinction increases almost linearly for aluminum and magnesium antennas. For copper a different behavior can be detected. Extinction increases first to peak at 17.12nm and decreases then until it reaches its lowest point at $T = 100\text{nm}$. Again peak position was determined by a polynomial fit.

Maximum extinction is strongly related to the electrical far-field. This only gives a hint on the behavior of electrical near-fields. Strong electrical near fields are needed for SEIRA. Since a strong maximum extinction was found for copper antennas, further research about their near-fields should be conducted. The shift in antenna resonance for copper antennas is stronger than for magnesium and especially for aluminum. But particularly for the gold film thickness of maximum extinction ($T = 17.12\text{nm}$) it is still small. It is about 14cm^{-1} which still is in an acceptable range for most applications.

Since no big shift of antenna resonance was detectable for aluminum when a gold film of changing thickness was added aluminum seems to be a good choice for surface en-

hanced infrared spectroscopy. In this way antenna tuning is not lost when the gold film thickness is varied due to the production process.

4.4 Au cap on Al, Cu and Mg antenna

In the following section simulation results of aluminum, copper and magnesium antennas coated with gold caps on their small sides will be presented. In the first part only the cap length l was varied while keeping the cap thickness T at a constant value. In the second part both parameters were changed.

4.4.1 Setup

In figure ?? a) a side view of the used simulation setup is shown. On top of a glass substrate (blue) the antenna (brown) is located. Around the edges of the antenna a gold cap of thickness T was added. The length of the cap that covers the antenna is annotated as l . The remaining setup as discussed in section ?? stayed unchanged. For antenna length L and periodicity Λ the optimized values from section ?? for a plasmonic resonance of 1200cm^{-1} were selected. A submesh grating of 5nm was chosen. As in prior simulations relative transmittance was measured. The source was located inside the substrate. All emitted light is polarized such that the electrical field component is oriented parallel to the antenna.

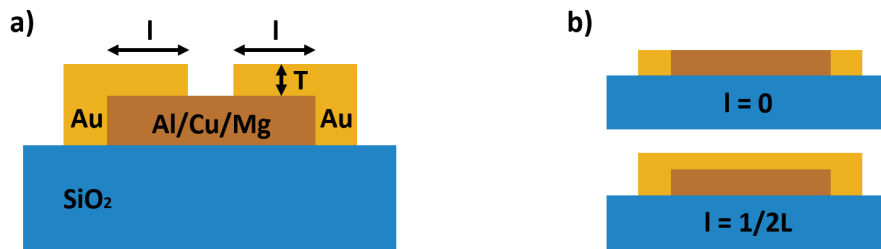


Figure 26: Side view of simulation setup for gold cap simulations. On top of a substrate (blue) a nanoantenna (brown) is located. On the small sides of the antenna a gold cap of thickness T and length l was added. l denotes the length the cap covers the antenna. b) Side view of $l = 0$ (only gold of thickness T on small sides) and $l = 1/2L$ (antenna fully covered).

4.4.2 Variation of length

Hereinafter, length l of the gold cap was varied for aluminum, copper and magnesium antennas. Both sides are varied at once resulting in a fully covered antenna when the cap length reaches a value of $l = 0.5L$. The behavior for a gold film thickness of $T = 50\text{nm}$ will be discussed here.

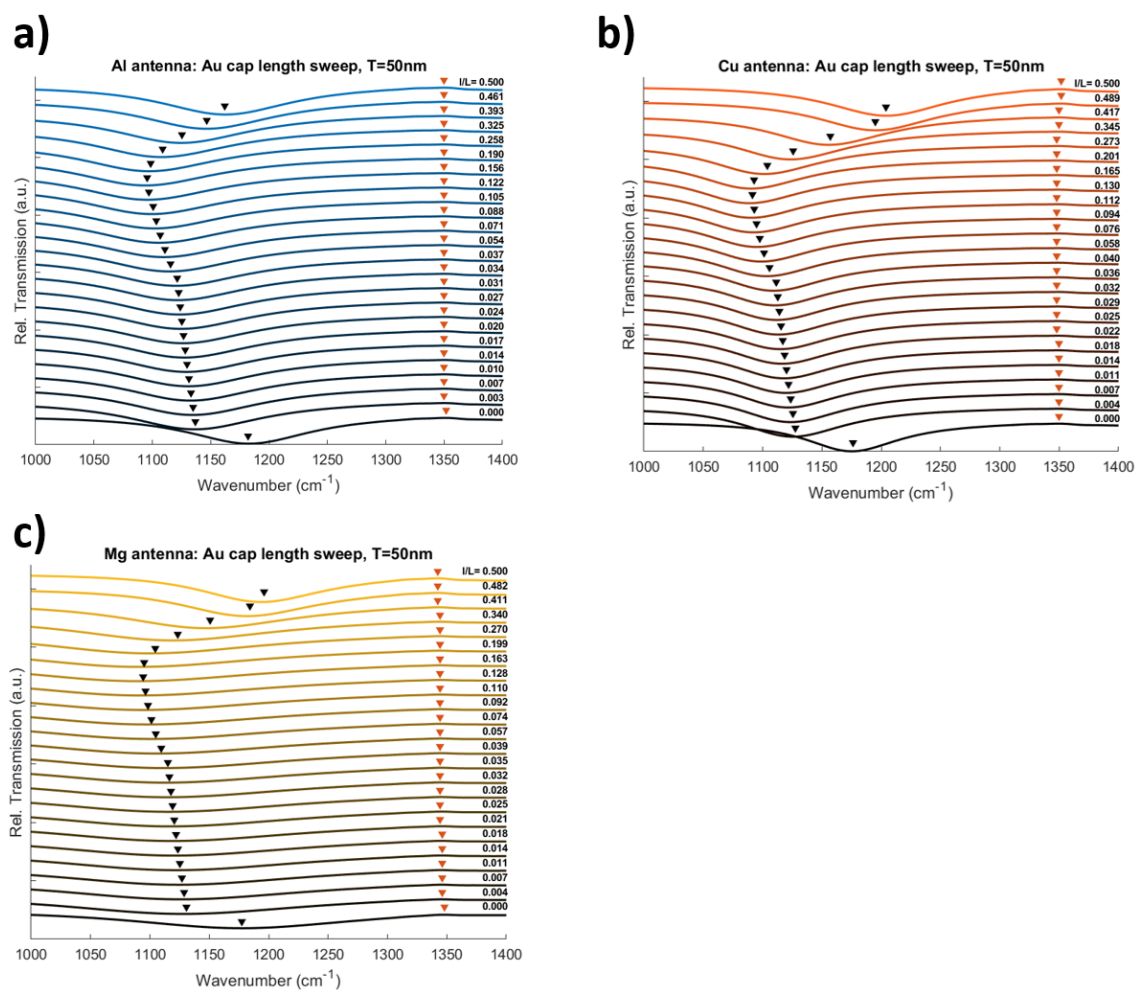


Figure 27: Simulation results for a length sweep from $l/L = 0$ (only small antenna sides are covered) to $l/L = 0.5$ (antenna fully covered in gold). The results are shown for different antenna materials. a) aluminum antenna b) copper antenna c) magnesium antenna. The ratio of au cap length versus antenna length is indicated by the legend. Plasmonic resonance and mesh resonance are plotted as black and red triangles.

In figure ?? the resulting spectra of a cap length sweep are plotted for different ratios of l/L . When a cap is added first a strong shift to lower wavenumbers can be observed for the plasmonic resonance. The shift decreases for higher ratios until it reaches a level of

about $l/L = 0.2$. Then plasmonic resonances are shifted to higher wavenumbers. Note that for all plots in figure ?? a constant offset was used. This offset does not correspond to the ratio l/L .

4.4.3 Variation of length and thickness

Results as shown in section ?? were obtained for gold cap thicknesses of $T = 10\text{nm}$, 20nm , 30nm , 40nm , 50nm , 80nm , 100nm for aluminum, copper and magnesium antennas. Simulation results will be discussed hereinafter. For each material the influence of gold cap thickness and cap length to plasmonic resonance was analyzed. The same was done for maximum extinction and full width of half maximum.

Gold cap length sweep on aluminum antennas In this paragraph measurements of a gold cap length sweep on a aluminum antennas will be discussed and analyzed.

In figure ?? the influence of a gold cap length sweep on various parameters of the aluminum antennas transmission spectrum is shown. In figure ?? a) the plasmonic resonance is plotted against the ratio of antenna length L and gold cap length l . This was done for different thicknesses T . As already seen in figure ?? a) a minimum in antenna resonance was found. The position of this minimum varies from $16.82\% L$ for $T = 100\text{nm}$ to $25.13\% L$ for $T = 10\text{nm}$. After its minimum the plasmonic resonance increases again for all thicknesses. Thereby it reaches a value that is even higher than without gold cap. Also the relative spans were included in the plot. They were calculated as

$$\frac{\omega_{max} - \omega_{min}}{\omega_{max}} \quad (30)$$

and range from 1.25% for $T = 10\text{nm}$ to 11.94% for $T = 100\text{nm}$.

In total it can be concluded that for high thicknesses the minimum of antenna resonance shows small values while its relative range is big. For small thicknesses the minimum of antenna resonance is located at higher values and its relative range is small. The minimal difference in plasmonic resonance is reached for fully covered antennas (around 60cm^{-1}).

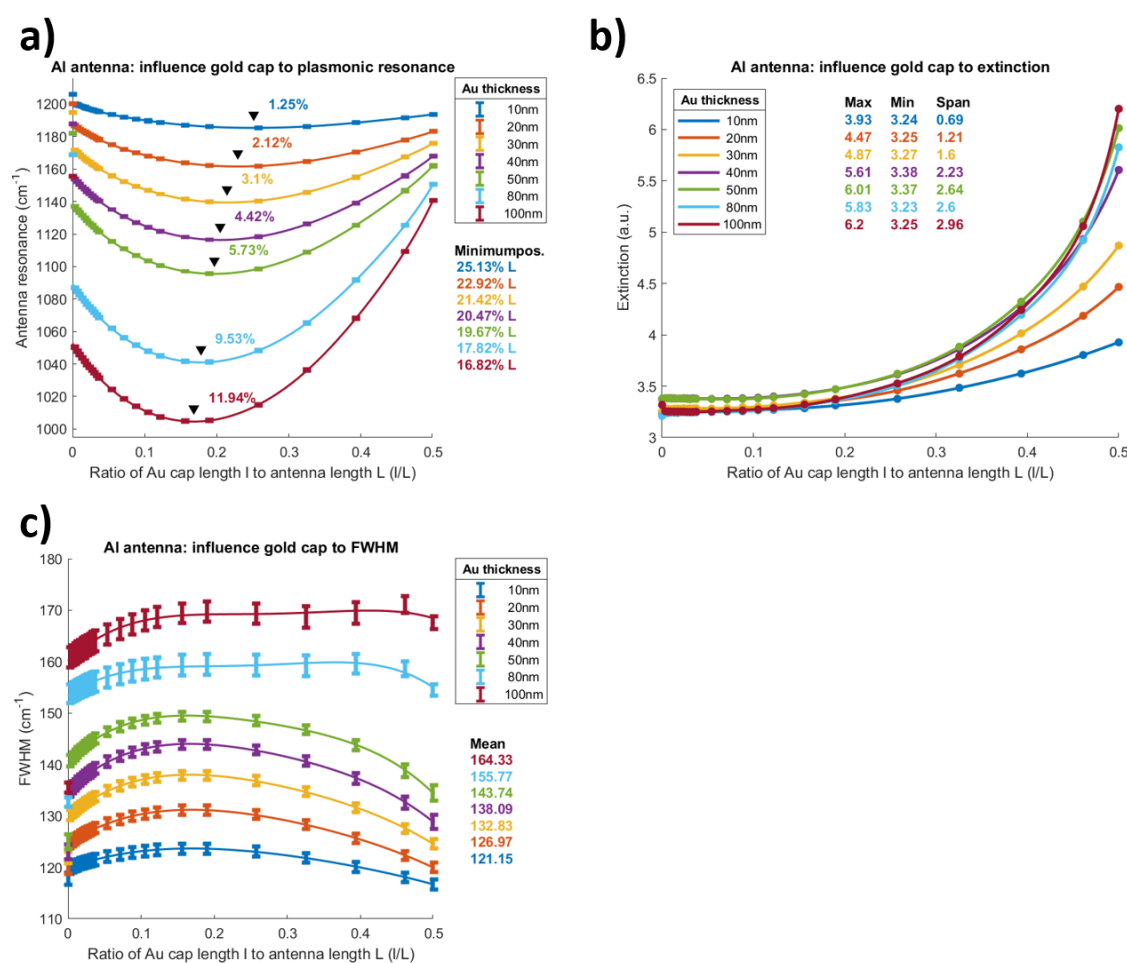


Figure 28: Influence of gold cap length and thickness sweep on different parameters of plasmonic resonance. An aluminum antenna was used. Fit errors are included. a) Influence of length sweep on plasmonic resonance position for different thicknesses T . Minimum position of each thickness is shown on the right and was marked by a black rectangle. Furthermore, resonance position span is shown in the plot. b) Influence of gold cap length sweep on maximum extinction for different gold cap thicknesses. Maximum and minimum extinction were added as well as the extinction span. c) Influence of length sweep on full width half maximum value. The mean was included and is shown on the right.

Gold and underlying antenna act as one material of strongly changed geometry. Since both materials are conducting they can interchange charge carriers. Boundary conditions for the interface of the two materials are changed as well, which has an additional effect on the spectral response. The changed geometry as well as modified boundary conditions are the reason for the behavior of antenna resonance, maximal extinction and full width half maximum value.

4. Results

In figure ?? b) the influence of a cap length sweep upon extinction was analyzed. This was done for all gold film thicknesses. Extinction was calculated using equation ??.

An increase in extinction was found for increasing cap length l . The higher gold cap thickness T the stronger extinction increases. For $l = 0\text{nm}$ extinction is almost constant for all thicknesses. With increasing length ratio L/l extinction increases too. Interestingly, extinction of $T = 50\text{nm}$ is generally higher than for $T = 80\text{nm}$ but lower than for $T = 100\text{nm}$. This might be due to some coupling effect of the gold and the underlying antenna material that is then compensated by the thick gold layer when the thickness reaches $T = 100\text{nm}$.

In summary, it can be pointed out, that a gold layer has an enhancing effect on an antennas extinction. This effect is stronger for increased gold cap thickness. For increasing cap length extinction also increases.

In figure ?? c) full maximum half width (FMHW) values extracted from the Lorentzian fits are presented. This was done for different gold cap thicknesses. Shown errors are fit errors.

For all thicknesses first an increase then a decrease in FMHW can be noticed. At a cap length ratio of around $l/L = 0.2$ the maximum is located. Only for higher thicknesses of $T = 100\text{nm}$ and $T = 80\text{nm}$ this maximum disappears. Both curves are almost constant with a derivation of around $\pm 10\text{cm}^{-1}$. Maximum derivation is reached for $T = 40\text{nm}$ of around 15cm^{-1} . In total derivation is small. Thus, for all curves of each T a almost constant FMHW was found. Therefore the mean was calculated and is also included in the graphic. The dependence of mean FWHM on gold cap thickness will be discussed in a later paragraph.

Gold cap length sweep on copper antennas In this paragraph the effects of a length sweep for gold caps on the plasmonic resonances of copper antennas will be discussed.

In figure ?? the influence of a gold cap length sweep on different parameters of the plasmonic resonance is shown. Just as for aluminum a dip can be found in plasmonic resonance behavior versus ratio of cap length. But other than for aluminum this dip is at a smaller and more constant position (from 14.86% L for $T = 100\text{nm}$ to 16.72% L for $T = 10\text{nm}$). Also the relative span is generally bigger for copper than for aluminum.

In figure ?? b) extinction dependence on gold cap length ratio is shown. Other than

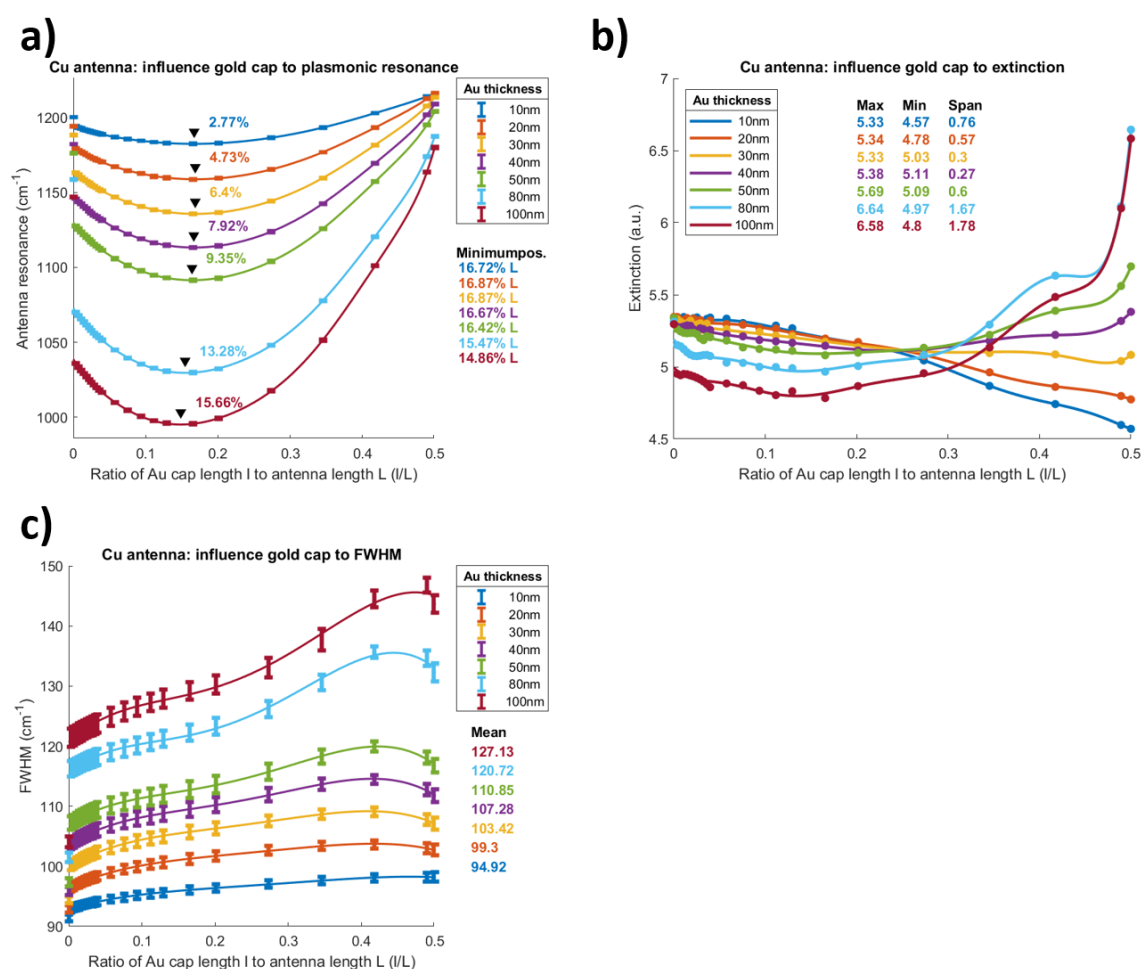


Figure 29: Influence of gold cap length sweep on different parameters of plasmonic resonance for a copper antenna. Figure setup similar to figure ??.

for gold only a small increase of extinction for higher thicknesses was found. For lower thicknesses even a small decrease is noticeable. For $T = 10\text{nm}$ to $T = 50\text{nm}$ extinction behaves almost linearly with continuously increasing slope from negative values for the lower thickness to positive values for the higher thicknesses. For higher thicknesses the behavior is similar to the one seen for gold capped aluminum antennas. For increasing length extinction increases as well. The span of extinction compared to aluminum is smaller.

In total an almost constant extinction was found for copper antennas coated with gold up to a thickness of $T = 40\text{nm}$. After that extinction strongly increases with increasing cap length.

In figure ?? c) FWHM in dependence of length ratio l/L is shown. Other than for gold an

4. Results

increase in FWHM up to about $l/L = 0.45$ can be noticed. After that FWHM decreases again. As for aluminum a small span (around 10cm^{-1}) was found for low thicknesses. For higher thickness FWHM shifts to higher values when length ratio is increased. The span is around 25cm^{-1} . A mean value was calculated and is featured in the plot.

Gold cap length sweep on magnesium antennas In this paragraph influence of a gold cap length sweep on magnesium antennas will be analyzed.

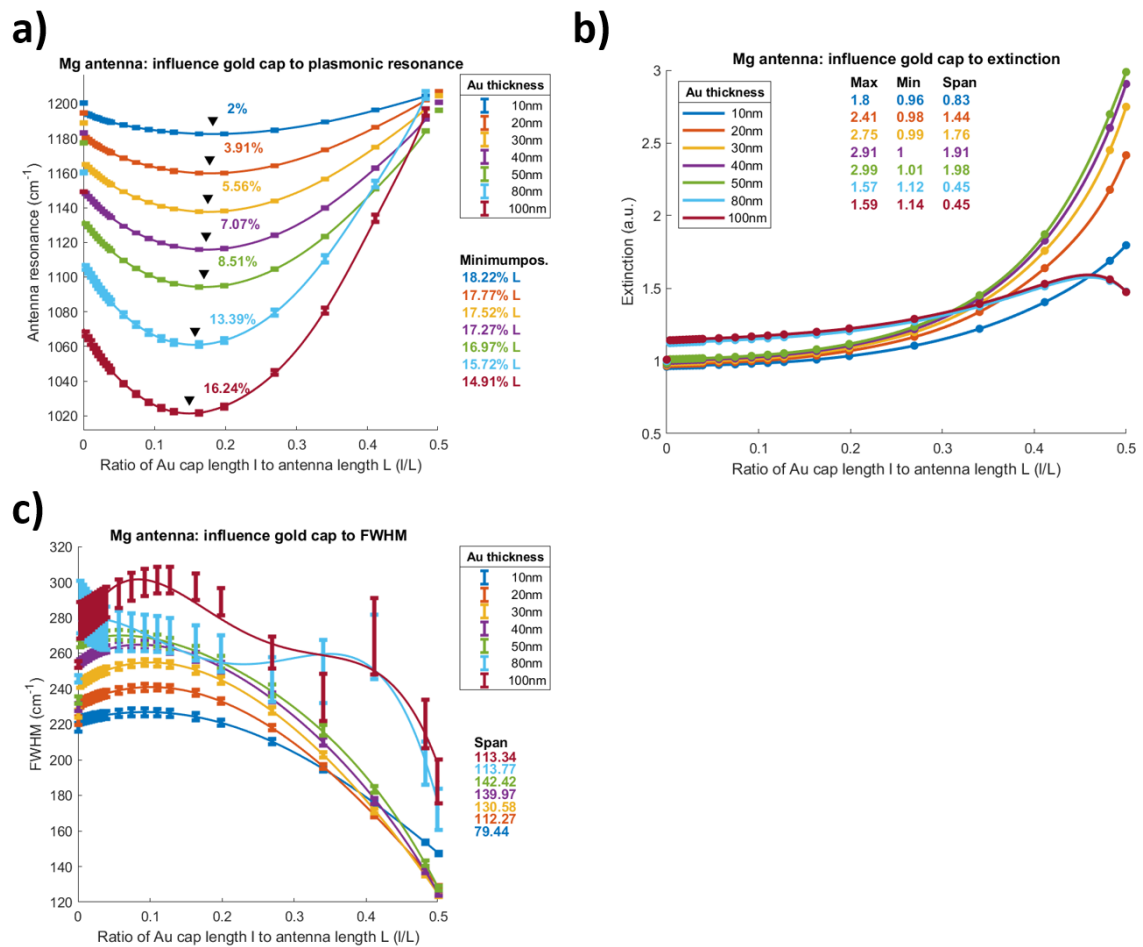


Figure 30: Influence of gold cap length sweep on different parameters of plasmonic resonance for a magnesium antenna. Figure setup similar to figure ??.

In ?? a) the plasmonic resonance position is plotted against antenna length ratio. As for aluminum and copper resonance is first decreasing to a minimum and then increasing to reach its maximum at $T = 100\text{nm}$. When fully covered all resonances are in a range of 10cm^{-1} . With a range from 14.91% for $T = 100\text{nm}$ to 18.22% for $T = 10\text{nm}$ the

minimum position is about the same as for copper. The range is a little higher than for copper and aluminum.

In total magnesium antennas resonance position is influenced the strongest when undergoing a gold cap length sweep.

In figure ?? b) extinction for different gold cap length ratios l/L is plotted. The shape of curves for thicknesses of 10nm to 50nm is roughly the same as for aluminum even though range as well as maximum extinction is smaller for magnesium antennas. But for higher thicknesses of $T = 100\text{nm}$ and $T = 80\text{nm}$ an abnormal behavior of extinction can be seen. For these curves maximum extinction increases first but starts decreasing again for a length ratio of about $l/L = 0.45$. This behavior might be caused by the high gold cap thickness that in this region is covering almost all of the antenna. Here, further simulations will be needed to find out the reason for this behavior.

In figure ?? c) FWHM for magnesium antennas in a gold cap length sweep is shown. Huge spans are detected and also featured on the right of the plot. Other than for copper and aluminum FWHM decreases strongly with increasing length ratio. Surprisingly the biggest difference between maximal FWHM and minimal FWHM is found for a thickness of $T = 50\text{nm}$. For higher thickness the span decreases slightly. As also seen in both cases before minimal span is reached for $T = 10\text{nm}$. No mean value was calculated. Instead the span is featured in the graphic.

In total for magnesium antennas FWHM is strongly gold cap length dependent.

Direct comparison In this paragraph a direct comparison of FWHM mean value versus gold cap thickness as obtained from above described simulations will be done.

In figure ?? the FWHM mean values for copper and aluminum antennas in dependence of gold cap thickness are shown. A linear dependence was found. Deviation of the featured χ_{red}^2 values to the perfect value of 1 are in the order of 10^{-3} and therefore very small. Thus, the fit can be evaluated to be good. Reason for the peak broadening could be the changed geometry of the antenna. Further research will be needed here.

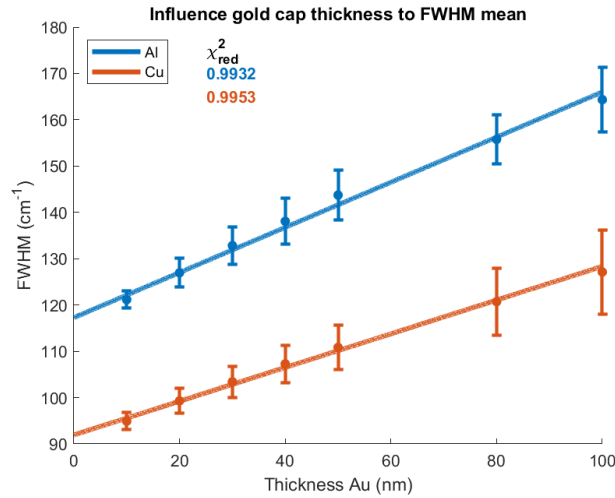


Figure 31: Dependence of FWHM mean value to gold cap thickness for copper and aluminum. Featured is also the standard derivation for each point. A linear fit was done which is also shown. Errors were weighted in. For evaluation of goodness of fit χ_{red}^2 values are featured for each fit.

4.5 FTIR result and comparison to simulated data

In this section results of FTIR measurements will be presented. Aluminum antennas of different length coated with gold were measured. Even though liftoff has already be performed some PMMA is still left and can be washed away by acetone bathing. Futhermore, a layer of Hexamethyldisiloxane (HMDS) was added between aluminum antenna and substrate. This setup will be used for functionalisation via DNA Origami to measure protein structures. Since a binding of DNA and protein to the substrate should be prevented, hydrophobic HMDS was added to repulse the hydrophilic DNA and protein.

The objective of those measurements was to determine the spectral response of this later used general setup. Also production should be checked via examination of the setup of the sample structure. A schematic drawing of the setup is shown in figure ???. As a substrate calcium fluorid (CeF2) was used.

Three samples were measured. Two of them coated with HMDS (sample 1 and 2), one without HMDS (sample 3). For On top of the aluminum antennas of varying length L a gold film of thickness $T = 4\text{nm}$ was coated. Futhermore, on all samples PMMA from production was left (see figure ?? a). For periodicity $p_x = 1000\text{nm}$ and $p_y = 3400\text{nm}$

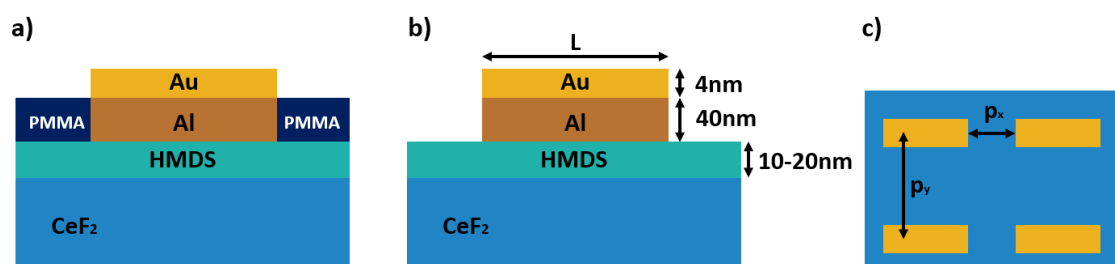


Figure 32: Setup of sample 1 and 2 as used for FTIR measurements. Sample 3 is missing the HMDS layer. a) Sample setup before acetone cleaning. PMMA from liftoff is still left. b) Sample setup after acetone cleaning. PMMA is removed. Used dimensions are also shown. Furthermore, a width of $W = 70\text{nm}$ was chosen. Other than before periodicity was defined as shown in c).

were chosen. Note, that p_x and p_y are defined differently than Λ as shown in figure ?? c).

After one measurement using FTIR all samples were put into a heated acetone solution for one hour. After that the acetone was renewed. This process was done three times to a total acetone bathing time of three hours for each sample. The samples then were cleaned using ultra pure water before carrying out the next measurement.

Using this method spectra similar to the ones shown in figure ?? were obtained. Here only small differences to the spectra of simulated nanoantennas were found. Therefore, the second derivative was calculated for each measurement and will be used for further analysis.

For each antenna length about 30 spectra were measured and averaged for analysis. All spectra shown also include a smoothed curve (blue). It was obtained by averaging over 10 data points.

4.5.1 General enhancement behavior

In this section the general enhancement behavior of nanoantennas as discussed in section ?? will be analyzed. Therefore, sample 1 was measured using the FTIR setup of the Pucci group before cleaning with acetone.

In figure ?? a) second derivative spectra of sample 1 are shown. Also all stronger vibra-

4. Results

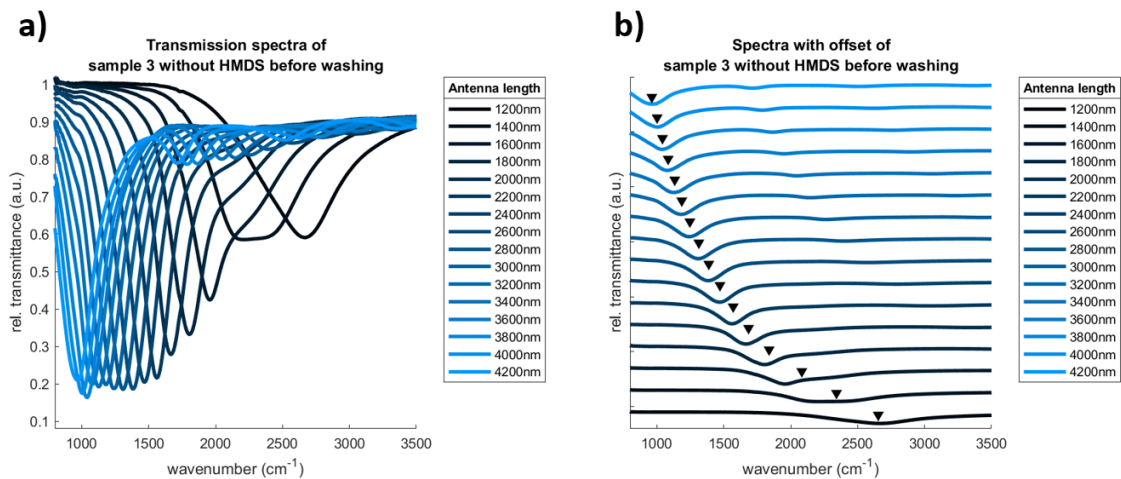


Figure 33: a) Relative transmittance spectrum for gold coated aluminum antennas of length as indicated by the legend. b) Same spectrum with offset. The antenna resonance is indicated by black triangles.

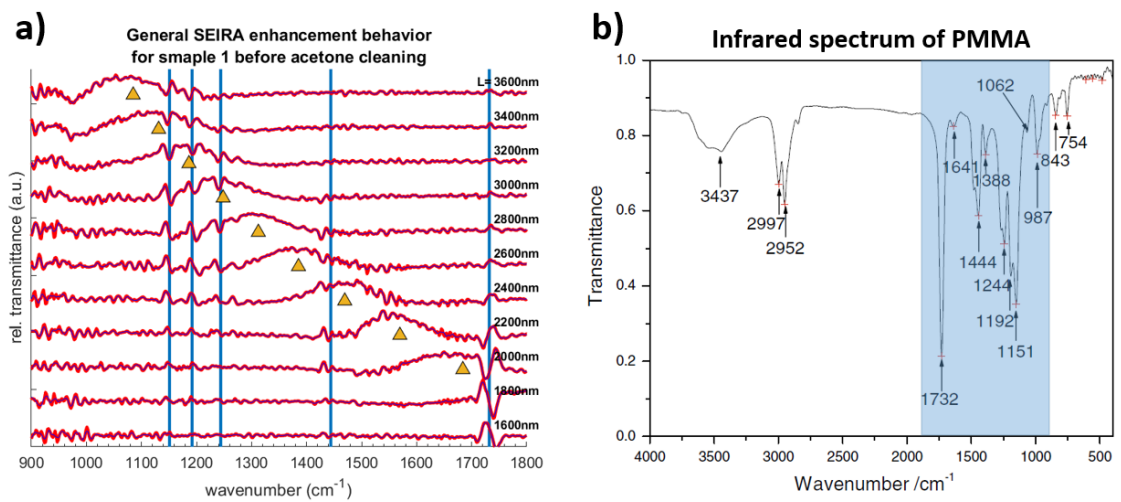


Figure 34: a) General SEIRA enhancement behavior. Second derivative of transmittance spectra of sample 1 before cleaning with acetone are shown for different antenna length as indicated by the legend. In blue vibrational frequencies of PMMA are shown. Also, antenna resonance position as obtained from Lorentzian fit are indicated by yellow triangles. b) IR spectrum of PMMA. The region of measurements was highlighted in blue. Graphic taken from [?]. Graphic was modified.

tional frequencies of PMMA (blue) are featured [?]. Antenna resonances as obtained from Lorentzian fits are indicated by yellow triangles. They are also visible as broad peaks in the spectrum.

A clear dependence of signal enhancement and antenna resonance position was found

for the PMMA signal. For example, focusing on the signal at the region around 1151cm^{-1} . The vibrational signal is clearly visible for antenna length of $L = 3600\text{nm}$ to 2200nm . For shorter length this signal becomes very small. Also when looking at the signal strength the highest values are obtained for length of 3200nm to 2800nm . This is exactly the range where plasmonic resonance and antenna resonance come close to each other. Another effect is the specific appearance of the resonance. For a match of antenna resonance and vibrational resonance a dip can be noticed. For an offset of these two frequencies first a dip then a peak is detected for $\omega_{\text{plasmon}} < \omega_{\text{vib}}$ and for $\omega_{\text{plasmon}} > \omega_{\text{vib}}$ a peak then a dip. This behavior is due to the coupling of the two resonances. The same behavior can be found in figure ???. For all vibrational frequencies the described behavior is detected. Especially the signal for 1072cm^{-1} is strong which is due to the strong vibrational band of PMMA at this frequency (see figure ?? b). In total a good signal of PMMA was obtained for this sample.

4.5.2 Analysis before and after acetone edging

In the following section FTIR results of sample 1 and 3 before and after cleaning with acetone will be presented.

Analysis of sample 1 (HMDS coated) In the first part results as obtained for sample 1 (HMDS coated) will be discussed. This sample is set up as shown in figure ?? a) before and as shown in b) after acetone edging. Possible signals for detection are respectively PMMA (only before edging), HMDS (before and after edging) and acetone (only after edging).

In figure ?? a direct comparison of spectra obtained before and after acetone washing is shown. Focusing on figure ?? a) one could reason that the seen signals are all due to PMMA since they are all located precisely around the blue lines. HMDS signals should be especially strong for 1175cm^{-1} and 1240cm^{-1} as well as 1440cm^{-1} . The signal at 1368cm^{-1} is very weak. For 940cm^{-1} only a signal for longer antennas would be detectable since they would be enhanced. In total it can not be determined for sure if the seen signals belong to HMDS or PMMA or a coupling of both.

In figure ?? b) the spectral response of sample 1 after acetone edging is shown. Spec-

4. Results

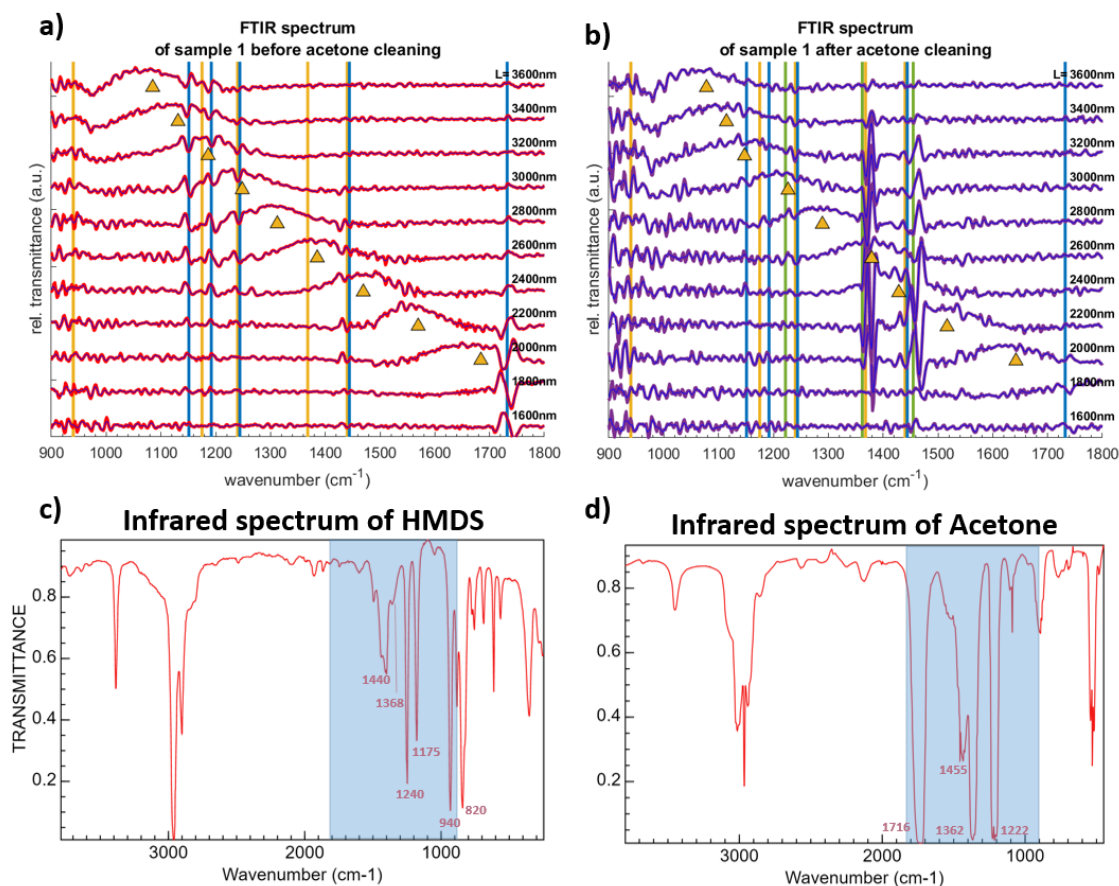


Figure 35: a), b) Direct comparison of second derivative of FTIR spectra of sample 1 before and after edging. Also, specific vibrational frequencies of PMMA (blue), HMDS (yellow) and acetone (green) are shown. c), d) Infrared spectra for HMDS and acetone as taken from [?]. The above shown spectral regions are highlighted in blue. Graphic was modified.

tral lines of acetone are added in green. Especially for wavenumbers around 1370cm^{-1} and 1440cm^{-1} a strong signal is detected due to the antenna enhancement. Surprisingly almost no signal is observable for a match of antenna resonance and vibrational frequency of 1370cm^{-1} . This might be due to coupling effects of the vibrational frequencies of HMDS, PMMA and acetone. Note, that both strong signals are exactly located at two of the strongest vibrational bands of acetone. Surprisingly no strong signal is found for the third strong vibrational band of acetone at 1222cm^{-1} . It therefore must be concluded that the strong signals are due to a coupling of HDMS, acetone and PMMA. PMMA probably plays a smaller role since its concentration should be significantly decreased after edging.

Focusing on the PMMA signals (blue) and comparing ?? b) to a) one can see that the signals especially at around 1135cm^{-1} and 1715cm^{-1} are significantly lower. This is due to the edging process where PMMA is cleared off the sample.

Analysis of sample 3 (no HMDS coated) In the second part results as obtained for sample 3 (no HMDS coated) will be discussed. Again sample design is as shown in figure ?? a) but without HMDS. Thus, potentially visible signals include only PMMA and acetone.

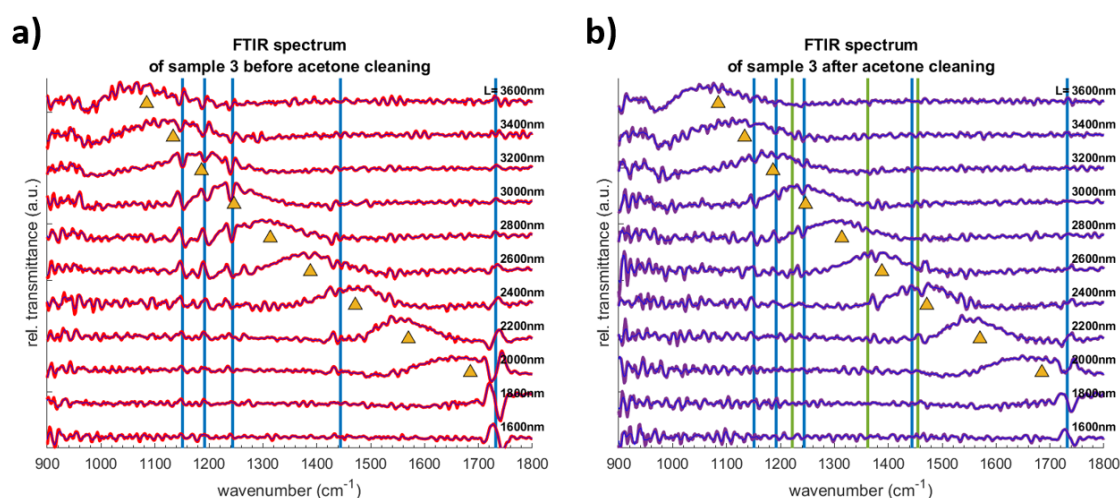


Figure 36: a), b) Direct comparison of second derivative FTIR spectra of sample 3 before and after edging. Figure setup similar to figure ??.

In figure ?? a) spectral response of sample 3 (no HMDS coated) is shown. The specific vibrational bands of PMMA are marked with blue lines. The obtained spectrum shows a variety of similarities to figure ?? a). Again all seen signals are precisely located at the vibrational bands of PMMA. Also an enhancement can be detected for $\omega_{\text{vib}} = \omega_{\text{plasmon}}$. This again gives a hint, that the HMDS signal in sample 1 before acetone cleaning is very weak.

In figure ?? b) FTIR results for sample 3 after acetone cleaning are presented. Spectral bands of acetone (green) and PMMA (blue) are marked. A decrease in PMMA signal strength can be seen. But also for acetone some small signals can be noticed. Especially a signal at 1455cm^{-1} is clearly visible. This signal is not detectable before washing although the PMMA concentration was higher. Hence, this signal must be due to acetone. The same can be pointed out for the signal at 1362cm^{-1} and 1222cm^{-1} even

4. Results

though both are very small.

Comparing the obtained spectra to the ones seen in figure ?? b) (sample with HMDS) big variations were found. The strong signal at 1360cm^{-1} and 1455cm^{-1} was not detectable any more. This means that assuming a comparable setup and treatment of both samples this resonance must be due to HMDS. Most likely it is a coupled resonance of mainly acetone, HMDS and some PMMA.

Summarizing it can be said that two strong signals were detected for sample 1 after acetone cleaning. These two resonances were traced back to a coupling of acetone, HMDS and PMMA. A good signal enhancement was visible for all measurements when plasmonic resonance and vibrational resonance were matched. It was found that even after acetone cleaning some PMMA signal was left. Hence, some PMMA is still remaining on the sample. This can be traced back to the fact that acetone is dissolving PMMA. Therefore some concentration of PMMA is always left in the acetone. When the sample is taken out of the acetone bath some of it remains at the surface and dries off. Even though ultra pure water was used to clean the sample a signal was still detectable. Thus, if elimination of PMMA signal is needed a new cleaning method should be considered. It is to mention that the effect of water cleaning and no water cleaning on the spectral response of these samples was analyzed in further measurements. No difference was detectable for the obtained spectra.

5 Summary

In this work nanoantenna behavior was investigated and tuned for application in surface enhanced infrared spectroscopy. Gold, aluminum, copper and magnesium nanoantennas were tuned for the vibrational frequencies of DNA, HMDS and a protein amide I group. The behavior of multilayer systems (gold on aluminum, copper or magnesium) was analyzed. All simulations were conducted using Lumerical FDTD Solutions.

In the first part of this thesis the enhancing effects of electrical near-fields for gold nanoantennas were investigated. A strong enhancement was found especially on both ends of the nanoantennas. Enhancement factors of 250 were reached. In the second part the typical spectral response of nanoantenna arrays were analyzed. Two resonances were visible: One belonging to the periodically arrangement (mesh resonance) and another to plasmonic excitations in the antenna (antenna resonance). The plasmonic resonance was determined as the minimum transmission using a Lorentzian fit. Mesh modes were obtained as the maximum relative transmission. Also a strong dependence of these resonances to periodicity (for mesh resonance) and antenna length (for antenna resonance) were found. A coupling of these two resonances was detected. It was the stronger the closer both resonances approached each other.

Tuning of resonances for SEIRA measurements of DNA, HMDS and a amide I protein group was done. Therefore, the mesh resonance was selected to be 150cm^{-1} above plasmonic resonance. The plasmonic resonance was tuned to match vibrational frequency of above mentioned materials. Performing an antenna length sweep a $1/L$ behavior of plasmonic resonance and antenna length was found. This result is according to Gans theory. For mesh resonance the deviation to the expected value was in the order of 10^{-2} . Both findings suggest a weak coupling of plasmonic and mesh resonance for the selected offset.

Simulations of multilayer systems (gold on aluminum, copper or magnesium) were performed. First a gold film covering the top of the antenna was considered. Thickness was varied during simulations. Plasmonic resonance and maximum extinction in dependence of gold film thickness were analyzed. A strong shift for antenna resonance was found for copper antennas. It increases with thickness and might be due to the higher total height of the multilayer system compared to a one material nanoan-

tenna. The same behavior was found for magnesium and aluminum antennas. Shifts were minimal for aluminum. Maximum extinction is maximal for copper and minimal for magnesium. Since for applications shifts in plasmonic resonance should be minimal, aluminum antennas seem to be a good choice for SEIRA. Also, a strong maximum extinction was found for aluminum and copper which gives a hint on a strong near-field enhancement. Here further research will be needed.

Multilayer systems of aluminum, copper and magnesium antennas enclosed with gold caps were analyzed. Gold cap thickness as well as enclosing length were varied. Plasmonic resonance, maximum extinction and full width half maximum were analyzed. With increasing enclosing length the shift in plasmonic resonance first decreases then increases. The minimum is located around 15 to 20% of the antenna length for all materials and cap thicknesses. The total span of resonance shift is the higher the thicker the gold cap is. Maximum extinction increases for aluminum and magnesium for increasing cap length. For copper this was only found for higher thicknesses. Full width half maximum is almost constant for each thickness for aluminum and copper. For magnesium it decreases strongly for increasing enclosing length. A linear relation for mean of full width half maximum and gold cap thickness was found for copper and aluminum antennas.

Using Fourier transform infrared spectroscopy spectral response of three samples was measured before and after acetone cleaning. The enhancing effect of SEIRA was analyzed using the signal of PMMA as an example. All samples processed aluminum antennas with coated gold. An analysis of the contained materials was done comparing the second derivative of relative transmission spectra to the vibrational bands of the materials. Two sample setups were measured: One containing HMDS the other one did not. When enhanced, the HMDS signal was visible. Furthermore, signals of PMMA and acetone were found.

Going forward, simulation results will be used for functionalization of DNA origami on top of the gold film. HMDS will be used as a repelling layer for the DNA on the substrate. Protein structures can be bound to DNA and measured using surface enhanced infrared spectroscopy. Changing DNA functionalization this setup enables the measurement of many other materials and therefore shows a wide range of applications in surface enhanced infrared spectroscopy.

References

- [1] STONE, J., JACKSON, S., WRIGHT, D.: Biological applications of gold nanorods. *WIREs Nanomedicine and Nanobiotechnology*, 3:100-109, 2011.
- [2] NEUBRECH, F., PUCCI, A., CORNELIUS, T. W.: Resonant plasmonic and vibrational coupling in a tailored nanoantenna for infrared detection. *Physical Review Letters* 101 (15), 2008.
- [3] HARTSTEIN, A., KIRTLEY, J. R.; TSANG, J. C.: Enhancement of the infrared absorption from molecular monolayers with thin metal overlayers. *Physical Review Letters* 45 (3), 1980.
- [4] NEUBRECH, F., HUCK, C., WEBER, K., PUCCI, A., GIESSEN, H.: Surface-enhanced infrared spectroscopy using resonant nanoantennas. *Chemical Reviews*, 117 (7), 2017.
- [5] WEBER, D.: Nanogaps for Nanoantenna-Assisted Infrared Spectroscopy. Dissertation, Ruperto-Carola-University of Heidelberg, Germany, 2011.
- [6] HUCK, Christian: Nanoantennenverstärkte Infrarotspektroskopie. Dissertation, Ruperto-Carola-University of Heidelberg, Germany, 2015.
- [7] ORDAL, M.A, R.J. BELL, R.W. ALEXANDER, L.L LONG und M.R. QUERRY: Optical properties of fourteen metals in the infrared and far infrared: Al, Co, Cu, Au, Fe, Pb, Mo, Ni, Pd, Pt, Ag, Ti, V, and W. *Appl. Opt.*, 24(24):4493–4499, 1985.
- [8] DRUDE, P.: Zur Elektronentheorie der Metalle. *Annalen der Physik*, 306(3):566–613, 1900.
- [9] PALIK, E.: *D. Handbook of optical constants of solids*, Academic Press: Cambridge, MA, Vol. 3, 1998.
- [10] *Journal of the Optical Society of America B*, Vol. 27, No. 4, April 2010.
- [11] MIE, G.: Beiträge zur Optik trüber Medien, speziell kolloidaler Metallösungen. *Annalen Der Physik*, 330(3), 377–445, 1908.
- [12] GANS, R.: Über die Form ultramikroskopischer Silberteilchen. *Annalen Der Physik*, 352(10), 270–284, 1912.

REFERENCES

- [13] LIAO, P.F, A. WOKAUN: Lightning rod effect in surface enhanced Raman scattering. *J. Chem. Phys.*, 76(1):751–752, 1982.
- [14] DUAN, G., ZHANG C., Li A.: Preparation and Characterization of Mesoporous Zirconia Made by Using a Poly (methyl methacrylate) Template, *Nanoscale Res Lett* 3:118–122, 2008.
- [15] SMITH, A.L., *The Coblentz Society Desk Book of Infrared Spectra* in Carver, C.D., editor, *The Coblentz Society Desk Book of Infrared Spectra*, Second Edition, The Coblentz Society:Kirkwood, MO, 1982, pp 1-24.

Acknowledgement

I want to thank Prof. Dr. Laura Na Liu for the opportunity to work within her group and perform the research, which led to this thesis, Prof. Dr. Yana Vaynzof for the co-examination, as well as Dr. Frank Neubrech for the supervision and discussion of the results. Furthermore, I would like to thank Prof. Dr. Annemarie Pucci for the opportunity to use her Fourier transform infrared spectrometer as well as Tianqiang Liu for the help when conducting the experiments. Also I want to express my thanks to the remaining group members for their various support. At the end, I want to thank my family and everyone that supported me during my thesis.

Erklärung

Ich versichere, dass ich diese Arbeit selbstständig verfasst und keine anderen als die angegebenen Quellen und Hilfsmittel benutzt habe.

Ort, Datum

Alexander Erb